

Evidências Experimentais

Sumário

I - Torneira Gotejante

II - Convecção de Rayleigh-Bénard

III – Fluido em Rotação

IV – Reação Química

I - Evidências Experimentais de Crises

Laboratório de Fenômenos Não Lineares

Principais autores dos trabalhos iniciais:

- J. C. Sartorelli
 - R. D. Pinto
 - W. M. Gonçalves
 - M. S. Baptista
-
- Pesquisas posteriores, desses e vários outros autores.

PHYSICAL REVIEW E

VOLUME 49, NUMBER 5

MAY 1994

Crisis and intermittence in a leaky-faucet experiment

J. C. Sartorelli, W. M. Gonçalves and R. D. Pinto

Instituto de Física, Universidade de São Paulo, Caixa Postal 20516, 01452-990 São Paulo, Brazil

Esquema do Equipamento

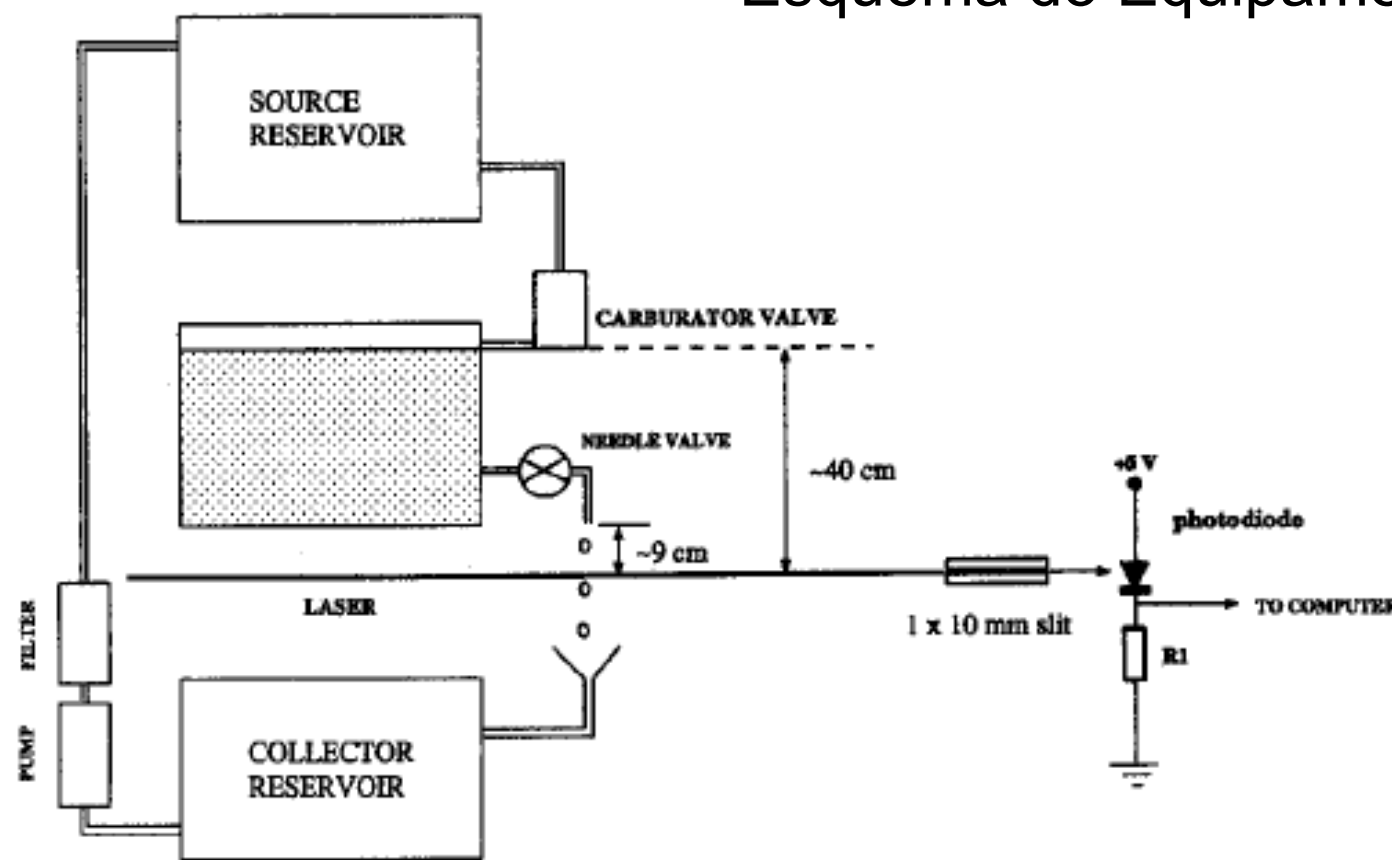


Figure 10.31 Diagram of the leaky faucet apparatus.

A carburetor valve is used to keep the main reservoir filled to a constant level, which holds the pressure at the needle valve constant. Drops are recorded when they break the laser beam which falls on the photodiode.

Chaos
Alligood et al.

Rota para o Caos (Duplicação de Período)

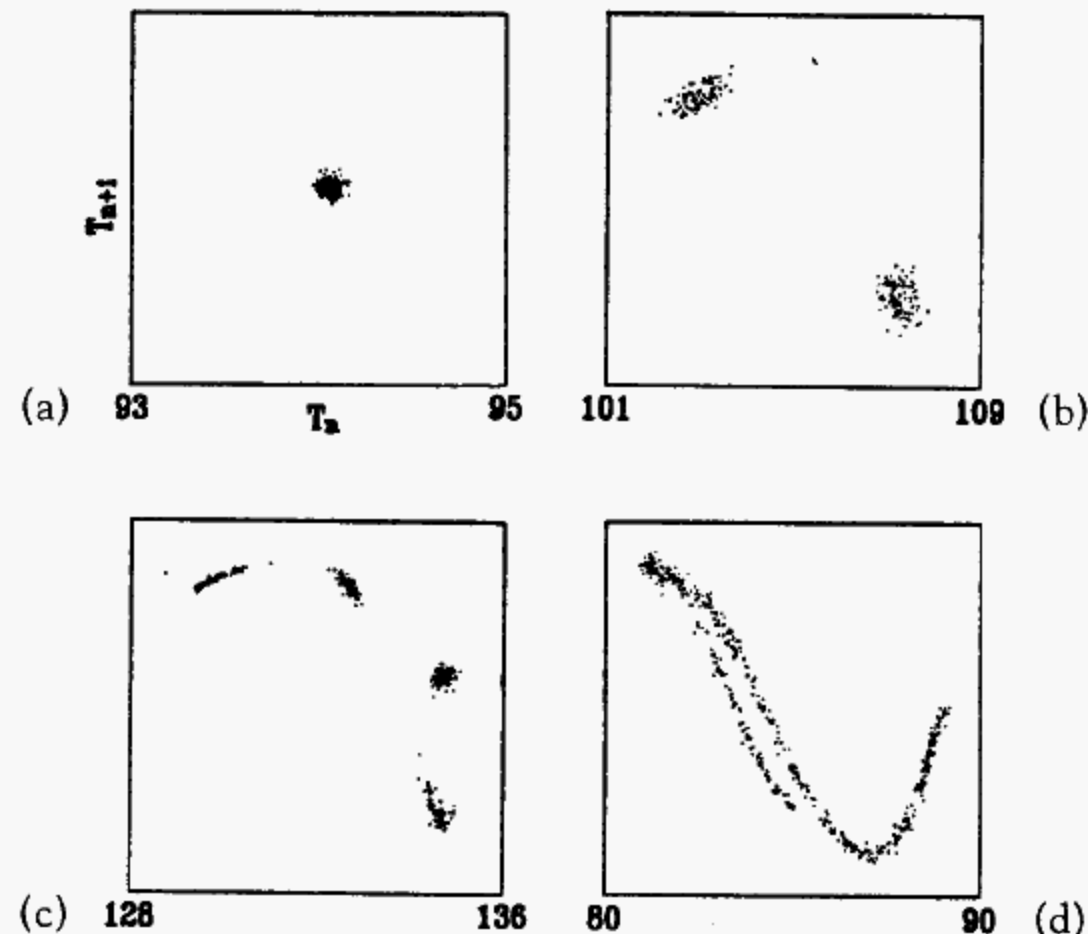


Figure 10.32 Scatter plots of successive interdrip intervals.

Pairs of form (T_n, T_{n+1}) are plotted. (a) Period-one. (b) Period-two. (c) Period-four. (d) Chaos.

Mapa de Retorno
do intervalo de tempo
entre duas gotas

Chaos
Alligood et al.

Diagrama de Bifurcação (Com Rotas para o Caos)

(Intervalos de tempo entre duas gotas)

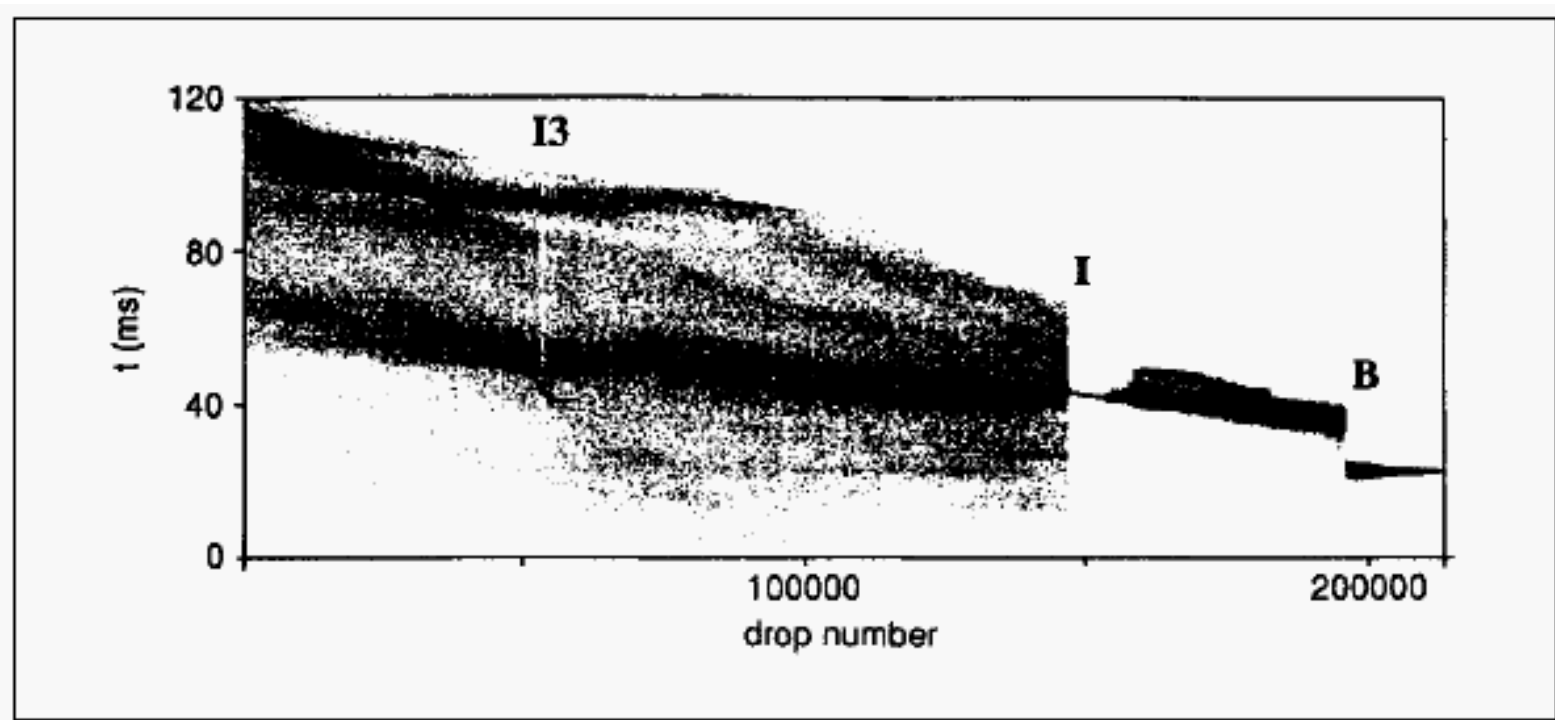


Figure 10.33 A bifurcation diagram for the leaky faucet.

Each vertical slice is 1024 dots corresponding to interdrip intervals. A period-three window (I3), an interior crisis (I), and a boundary crisis (B) are identified.

Mudança de Atrator (Crise interior indicada por I no diagrama de bifurcação)

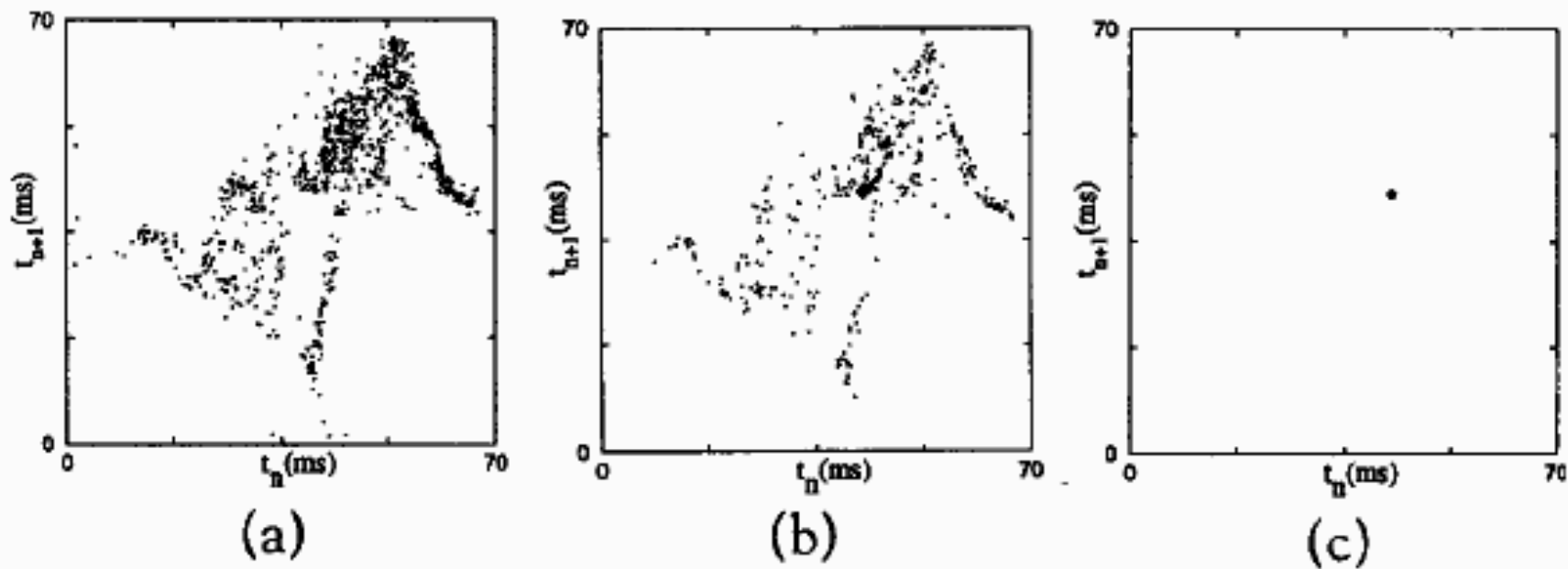


Figure 10.34 Scatter plots of successive time-interval pairs near the interior crisis.

(a) Complicated dynamics before the crisis parameter value I is followed by simpler dynamics in (b) and (c) as the flow rate is slowly increased.

Crise de Fronteira (indicada por B no diagrama de bifurcação)

Atrator caótico

Atrator com período 5

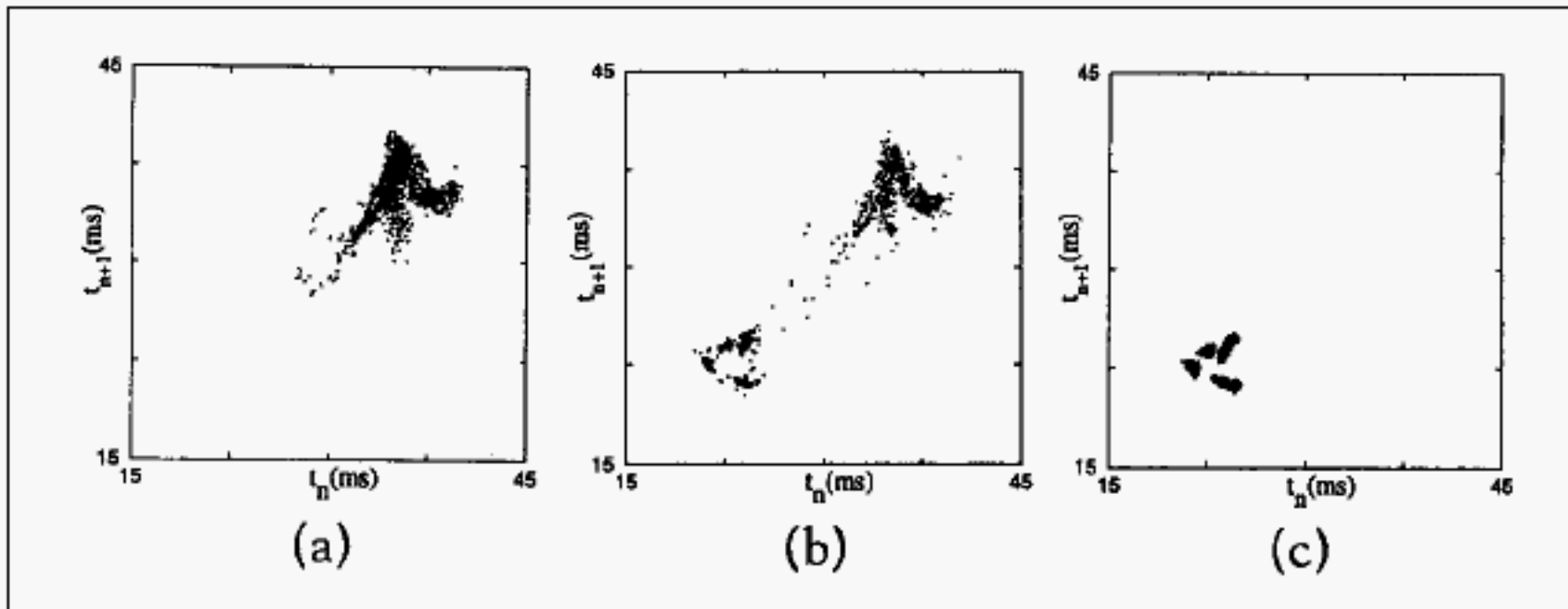


Figure 10.35 Scatter plots near a boundary crisis.

(a) Complicated dynamics before the transition yields to periodic behavior as the basin boundary of the original attractor is destroyed in (b) and a periodic attractor results in (c).

Transição caos→ periódico

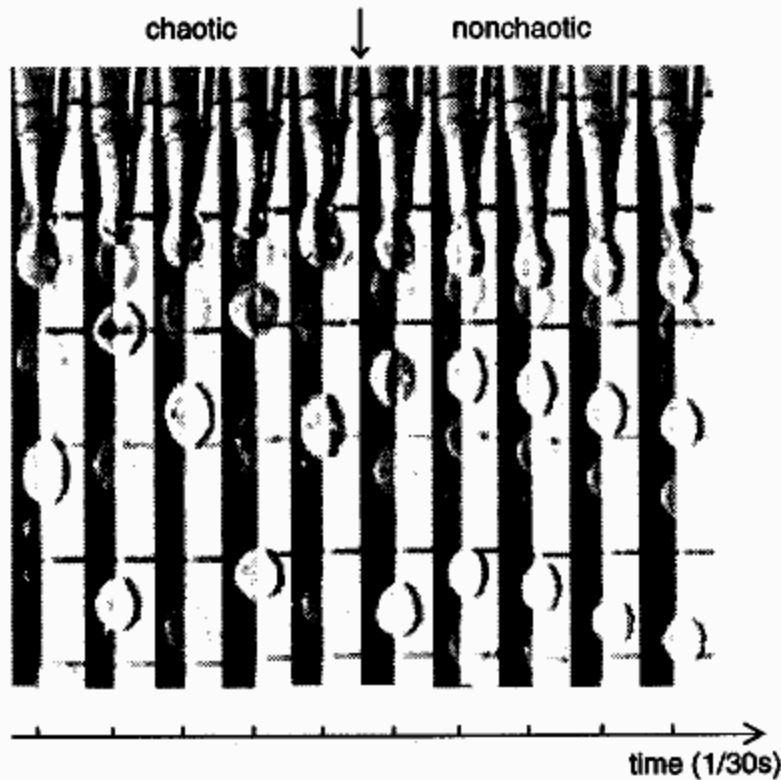


Figure 10.36 Transition from chaotic to periodic pattern.

A motion picture recorded at 30 frames per second shows the change from chaotic (first five frames) to period-five (last five frames) behavior.

Chaos
Alligood et al.

PHYSICAL REVIEW E

VOLUME 61, NUMBER 1

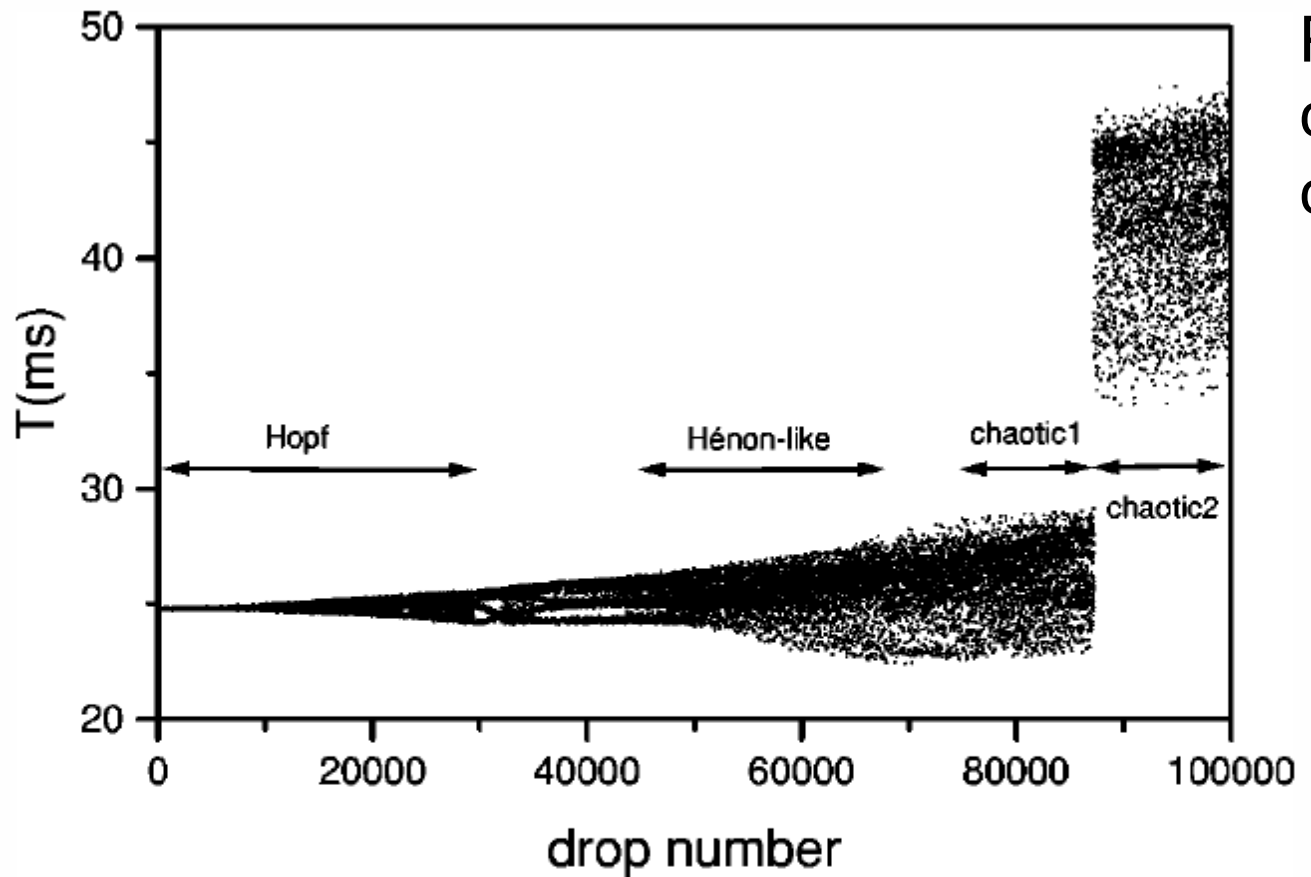
JANUARY 2000

Homoclinic tangency and chaotic attractor disappearance in a dripping faucet experiment

Reynaldo D. Pinto* and José C. Sartorelli†

Instituto de Física, Universidade de São Paulo, Caixa Postal 66318, 05315-970 São Paulo, SP, Brazil

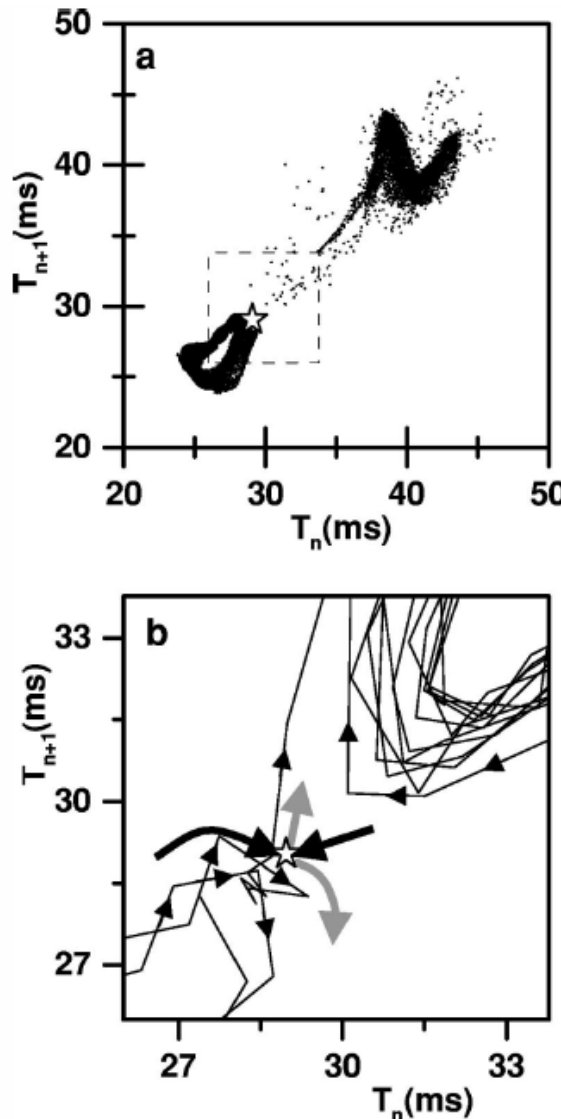
Diagrama de Bifurcações



Ponto fixo →
ciclo limite →
caos

Mudanças no
atrator caótico

FIG. 1. Bifurcation diagram obtained by letting the water level of a 501 reservoirs decrease naturally with the dripping. The time series $\{T_n\}$ is 100 000 drops long, but we plotted just one point every four to let the figure clear.

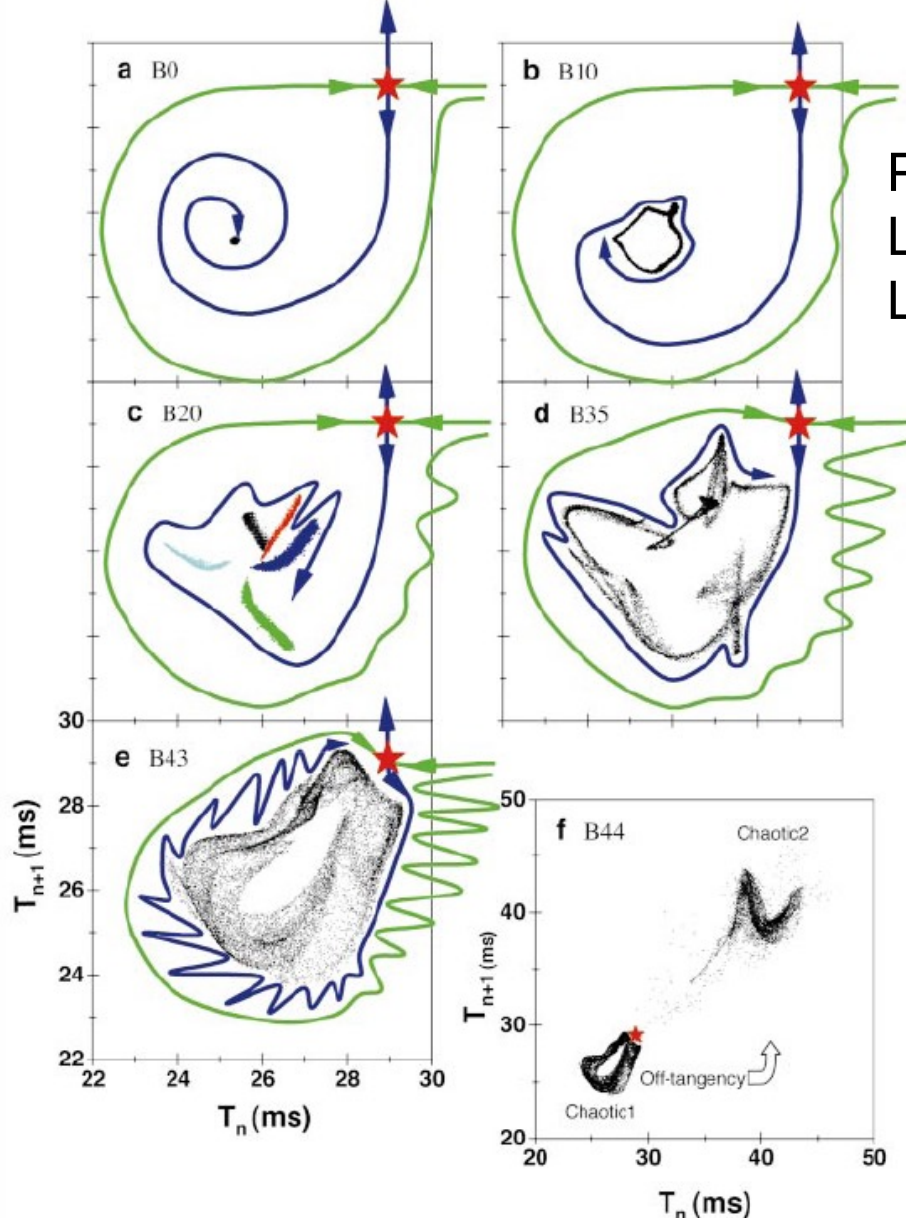


Transiente Caótico

Ponto de Sela

Variedades

FIG. 2. (a) First return map of the transient subseries B44. (b) Enlarged view of the square region above. The saddle point S1 at ($\sim 29 \text{ ms}$, $\sim 29 \text{ ms}$) is represented by a star. The gray (black) lines are pictorial representations of the local unstable (stable) manifolds. The saddle point and its manifolds were inferred following the orbits represented by the smaller black arrows.



Ponto vermelho: sela
 Linha azul: variedade instável da sela
 Linha verde: variedade estável da sela

Transição
 Fig. e → Fig. f

atrator cruza variedade
 estável e sofre expansão

FIG. 7. (Color). Evolution to a blue sky catastrophe by following the first return maps as a function of the faucet closing. All graphs are the same scale, except the last one. The red star represents the saddle point S1, the blue (green) lines are pictorial representations of the unstable (stable) manifolds suggested by the orbits and the dynamical evolution. (a) a stable focus. (b) a torus in the Hopf region and the ginning of the representation of the folds due to the torus enlargement that pushes the unstable manifold toward the stable one. (c) a Hénon-like attractor generated by the tangency of the torus with the unstable manifold. (d) the first attractor in the chaotic 1 region and in (e), the last chaotic 1 attractor where the manifolds are close to the tangency. In (f), with the off-tangency of the manifolds the orbits migrate to the new chaotic 2 region, characterizing a chaotic blue sky catastrophe.

PHYSICAL REVIEW E

VOLUME 58, NUMBER 3

SEPTEMBER 1998

Interior crises in a dripping faucet experiment

R. D. Pinto,* W. M. Gonçalves, J. C. Sartorelli,[†] and I. L. Caldas

Instituto de Física da Universidade de São Paulo, Caixa Postal 66318, 05315-970, São Paulo, SP, Brazil

M. S. Baptista

Institute for Physical Science and Technology, University of Maryland at College Park, College Park, Maryland 20742

Duas Crises Interiores

- a) antes da primeira crise
- b) c) entre primeira e segunda crise
- d) após segunda crise

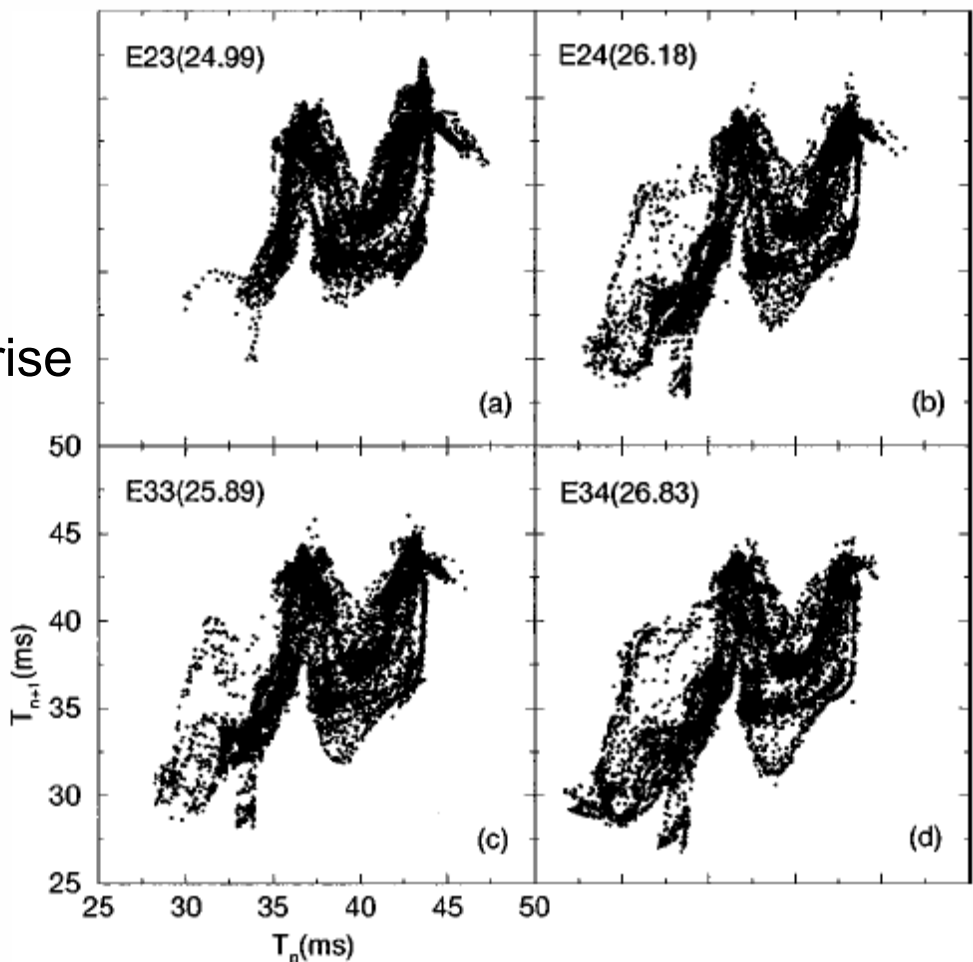


FIG. 1. First return maps T_{n+1} vs T_n representing three identified groups of attractors. (a) belongs to the group before the first interior crisis, (b) and (c) belong to the group between the first and the second interior crises, and (d) belongs to the group after the second crisis. The numbers in parenthesis are the dripping rates.

Sucessão de Regimes Crises Interiores

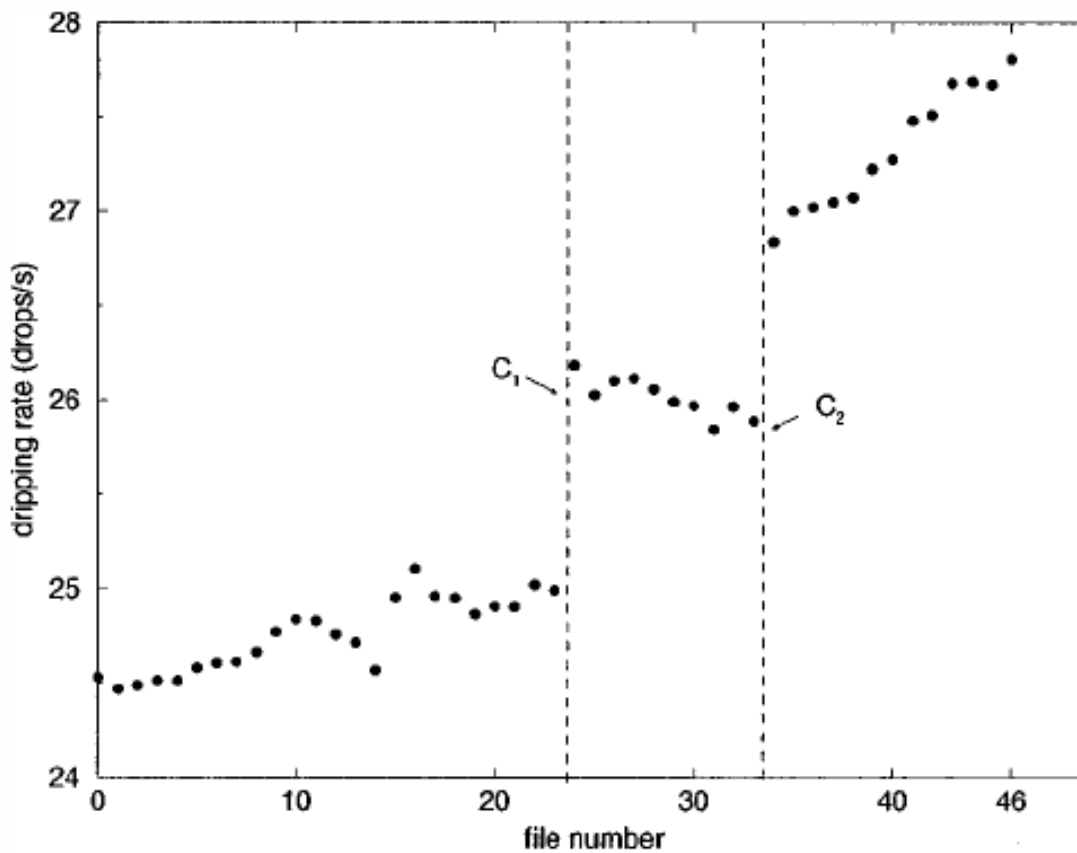


FIG. 2. Dripping rate as a function of file number (faucet opening). The sudden changes in the dripping rate (C_1 and C_2) correspond to the first and second interior crises.

II – Evidência Experimental de Crise

Convecção de Rayleigh-Bénard

is the temperature difference between the bottom and top plates). The natural control parameter is the *Rayleigh number* defined as:

$$R = \frac{\alpha g \Delta T h^3}{\kappa \nu},$$

where α is the expansion coefficient and g the acceleration of gravity. The thermal diffusivity κ and the kinematic viscosity ν parameterize the stabilizing dissipative processes. The last parameter that shows up in these dimensionless equations is the Prandtl number $P = \nu / \kappa$ that controls the nature, either mostly thermal or

We employ the *Boussinesq approximation*: density perturbations affect only the gravitational force.

The momentum equation is therefore the Navier-Stokes equation augmented by the buoyancy force:

$$\frac{\partial \vec{u}}{\partial t} + \vec{u} \cdot \vec{\nabla} \vec{u} = -\frac{1}{\rho_0} \vec{\nabla} p + \nu \nabla^2 \vec{u} - \vec{g} \alpha (T - T_0)$$

Here we have written the *kinematic viscosity*

$$\nu = \eta / \rho_0$$

The mass conservation equation is again

$$\vec{\nabla} \cdot \vec{u} = 0.$$

We now additionally require an equation for the convection and diffusion of heat:

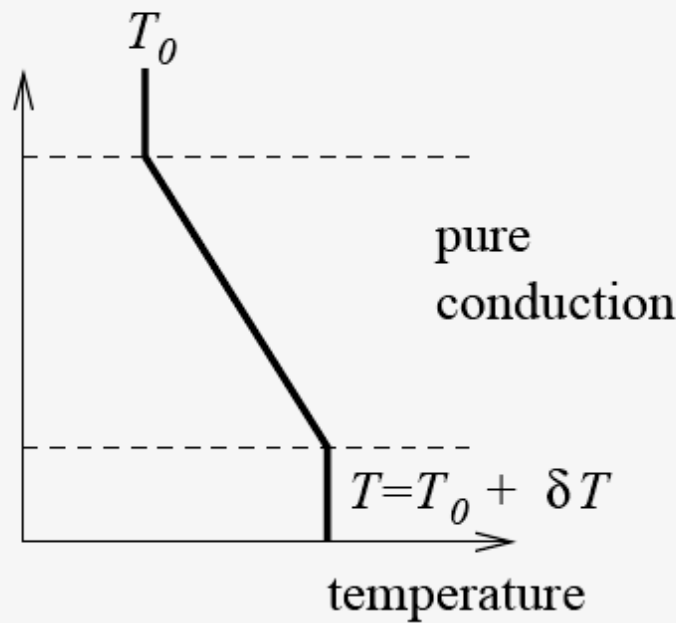
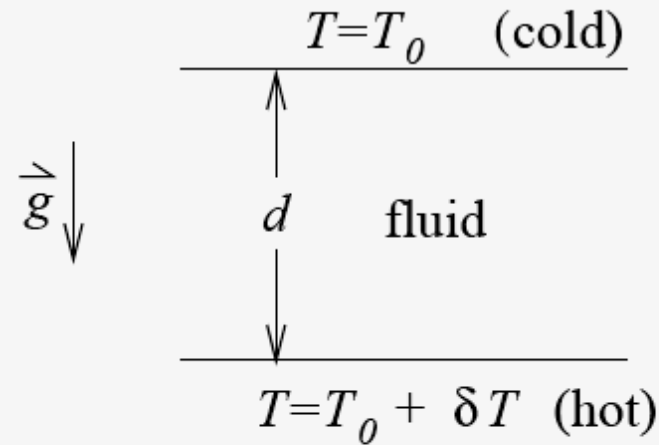
$$\frac{\partial T}{\partial t} + (\vec{u} \cdot \nabla) T = D_T \nabla^2 T.$$

9.5 Rayleigh-Bénard convection

In a thermally expansive fluid, hot fluid rises.

R-B convection concerns the study of the instabilities caused by rising hot fluid and falling cold fluid.

Typically,, fluid is confined between two horizontal, heat-conducting plates:



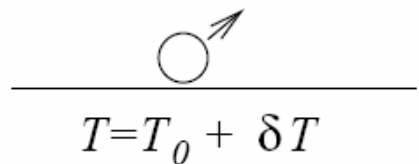
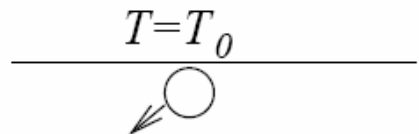
In the absence of convection—the transport of hot fluid *up* and cold fluid *down*—the temperature gradient is constant.

Two cases of interest:

- δT small: no convective motion, due to stabilizing effects of viscous friction.
- δT large: convective motion occurs.

The buoyancy force is resisted by viscous friction between the two blobs separated by $\sim d$.

Consider a small displacement of a cold blob downwards and a hot blob upwards:



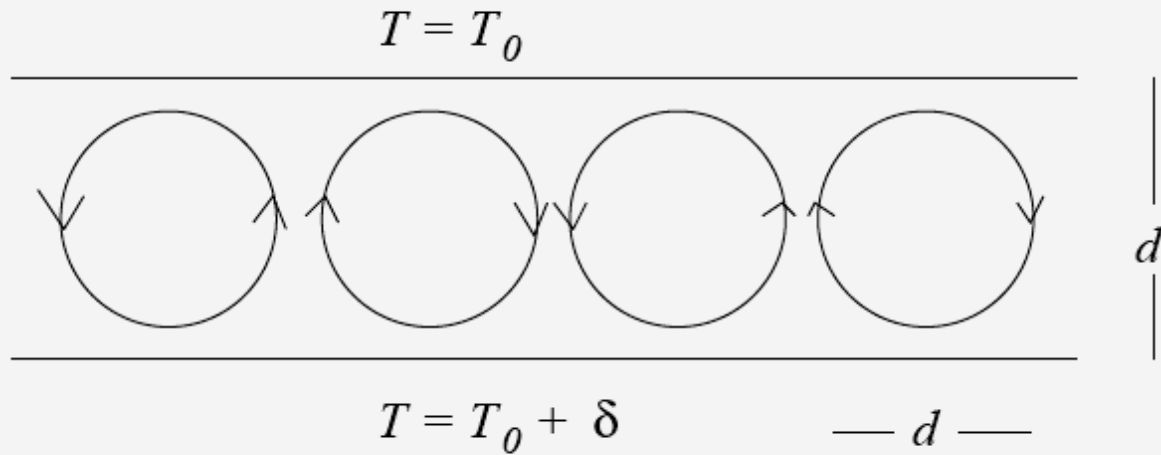
Left undisturbed, buoyancy forces would allow the hot blob to continue rising and cold blob to continue falling.

There are however damping (dissipation) mechanisms:

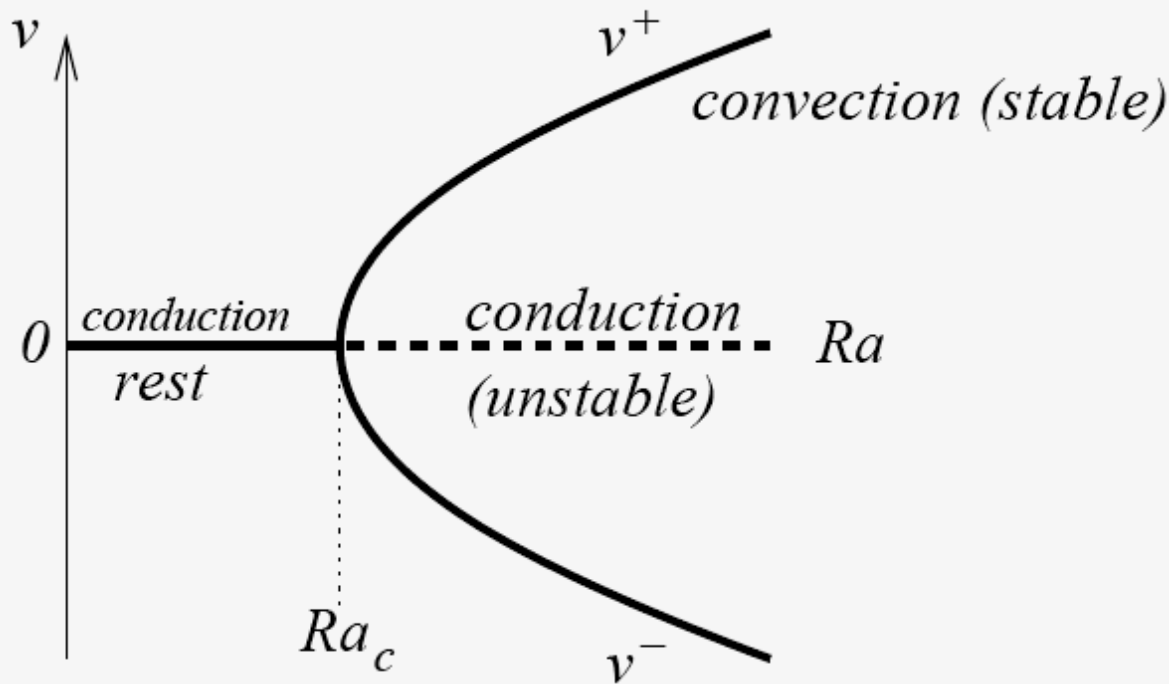
- diffusion of heat
- viscous friction

For $\text{Ra} < \text{Ra}_c$, there is no convection.

For $\text{Ra} > \text{Ra}_c$, but not too large, a regular structure of convection “rolls” forms, with hot fluid rising and cold fluid falling:

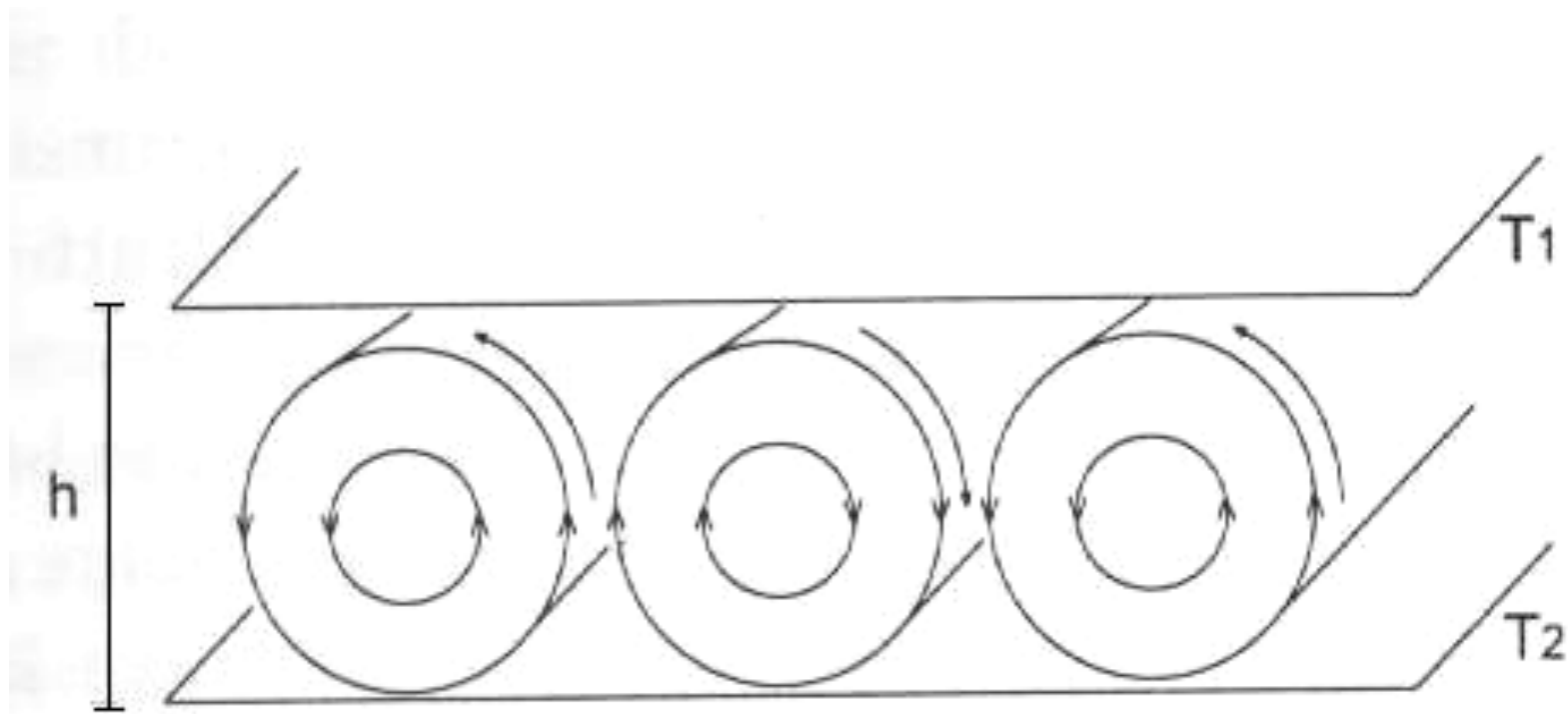


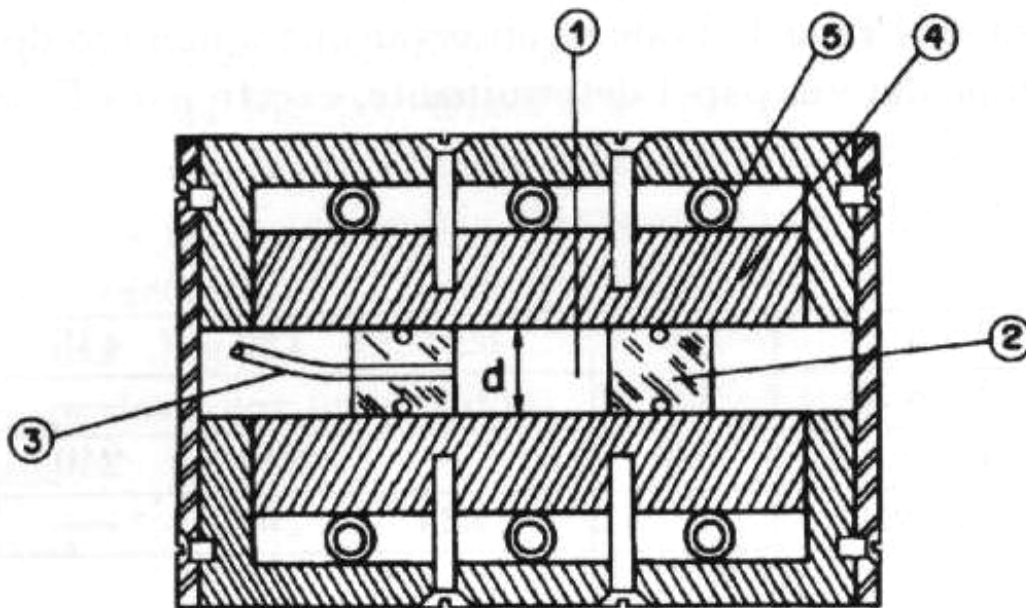
Now imagine placing a probe that measures the vertical component v of velocity, somewhere in the box midway between the top and bottom. A plot of $v(\text{Ra})$ looks like



Such a plot is called a *bifurcation* diagram. Here the stable states are bold and the unstable states are dashed.

Note that we cannot know in advance whether the velocity will be up or down. This is called *symmetry breaking*.





Esquema do dispositivo para estudo da convecção de Rayleigh-Bénard. 1 – Cavidade do fluido, 2 – peças de “plexiglass” que definem a cavidade, 3 – tubo para introdução do fluido, 4 – placas de cobre, 5 – tubos para água (banho termostático).

Numerical Solutions

Equação de Navier-Stokes

$$\rho \frac{d\vec{v}}{dt} = \vec{F} - \vec{\nabla}p + \mu \nabla^2 \vec{v}$$

$$\frac{dT}{dt} = K \nabla^2 T$$

Equação de Condução do Calor

Equação da continuidade

$$\frac{\partial \rho}{\partial t} + \vec{\nabla} \cdot (\rho \vec{v}) = 0$$

Equações de Lorenz

$$\frac{dX}{dt} = -\sigma(X - Y)$$

$$\frac{dY}{dt} = rX - Y - XZ$$

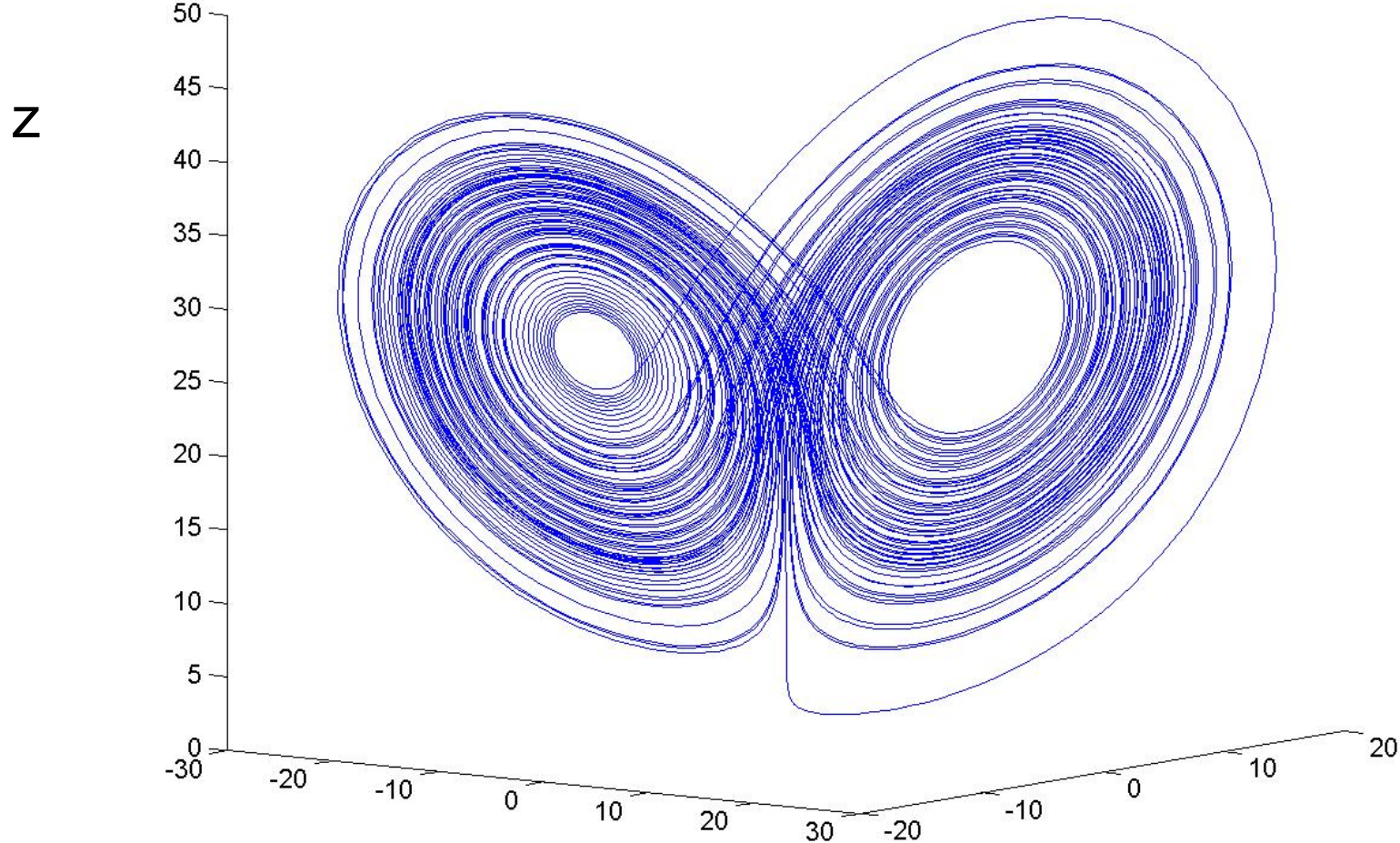
$$\frac{dZ}{dt} = XY - bZ$$

X é proporcional à intensidade da convecção. X=0 implica que não há movimento convectivo, ou seja, o calor é transportado apenas por condução. X>0 implica circulação horária e X<0 circulação anti-horária.

Y é proporcional à diferença de temperatura entre as correntes de fluido ascendente e descendente.

Z é proporcional à distorção do perfil de temperatura vertical, relativamente a um perfil linear. Para Z=0, a temperatura decresce linearmente.

Atrator de Lorenz



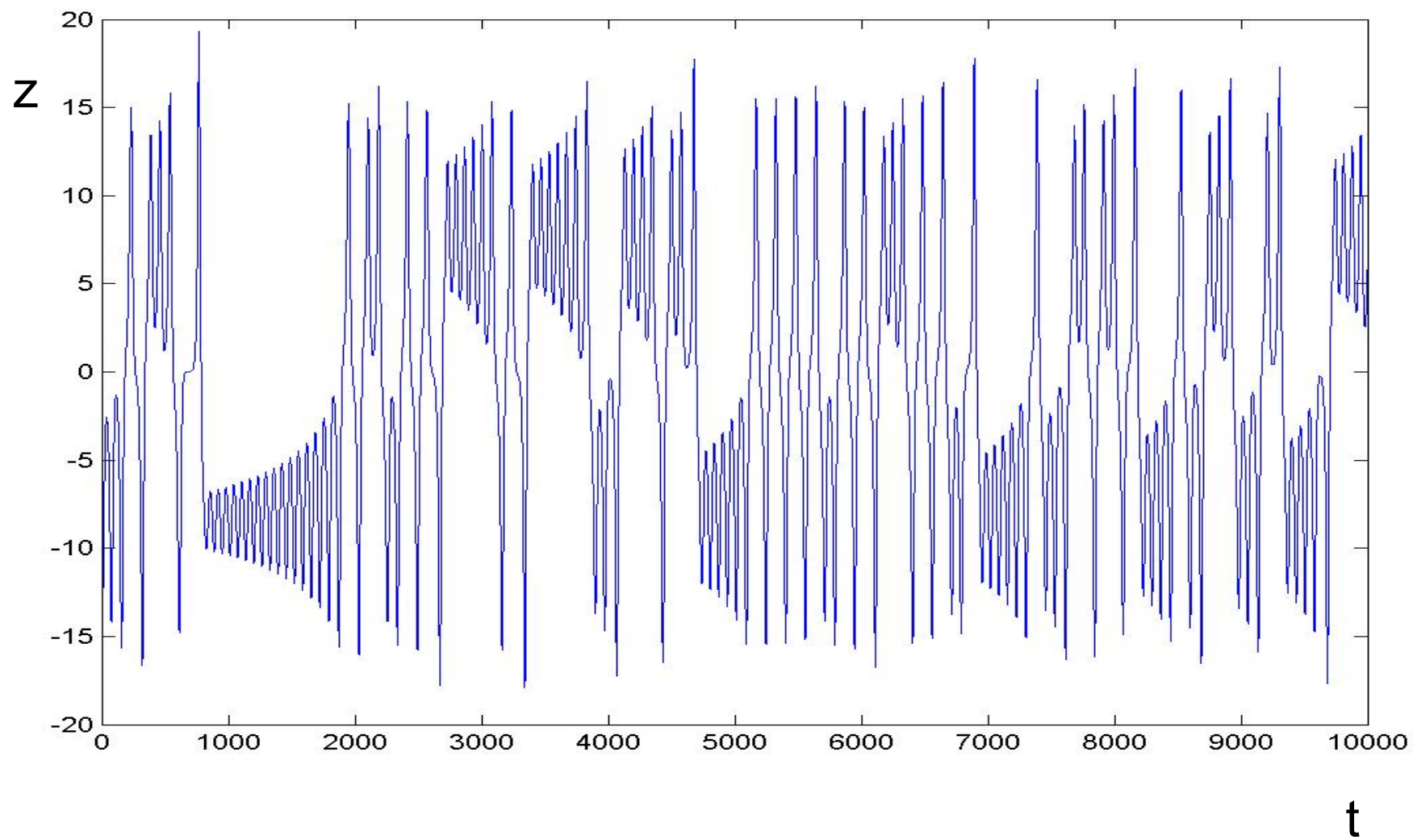
$$\sigma = 10$$

$$b = 8/3$$

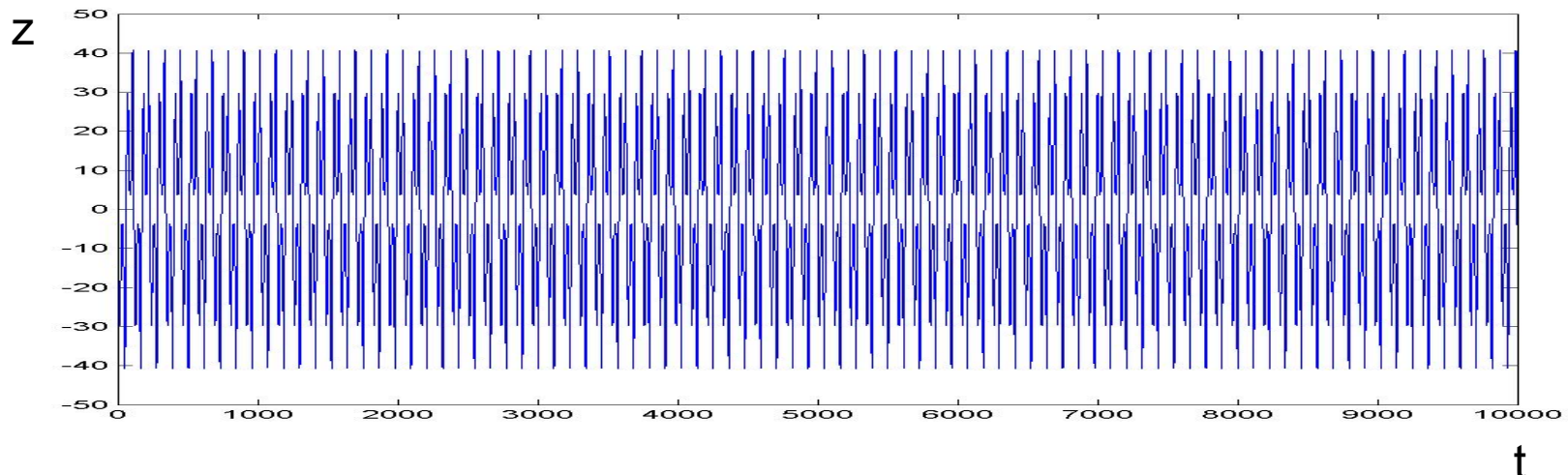
$$r = 28$$

Evolução da Variável Z

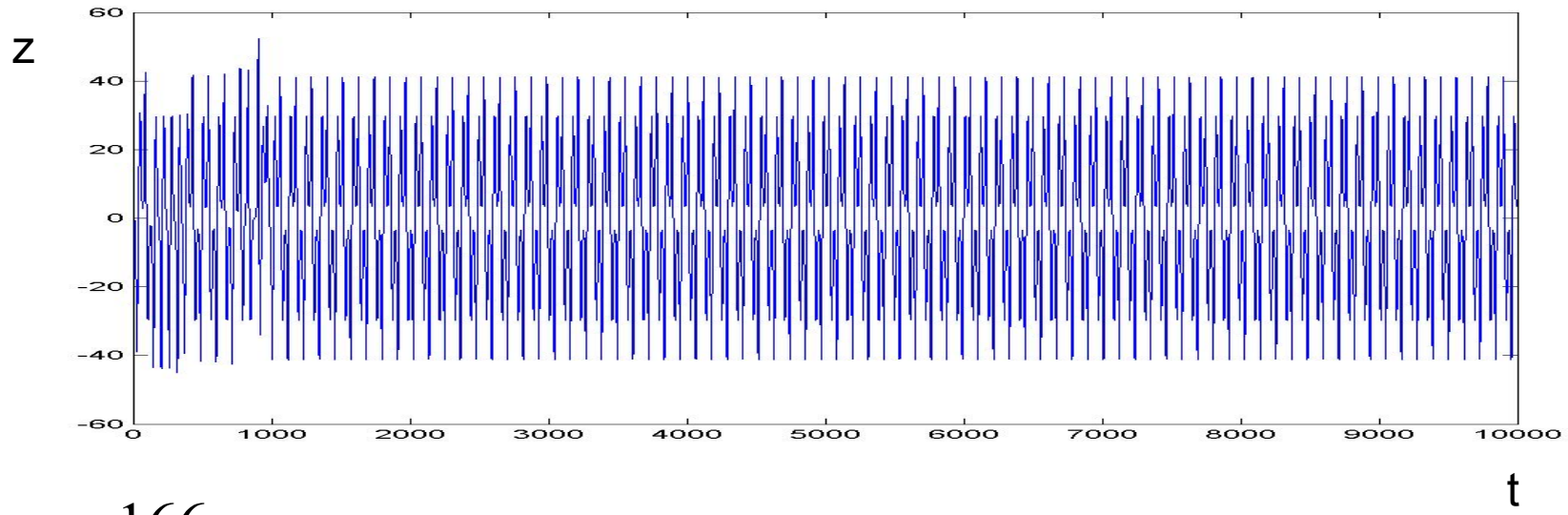
Atrator Caótico



Atratores Periódicos

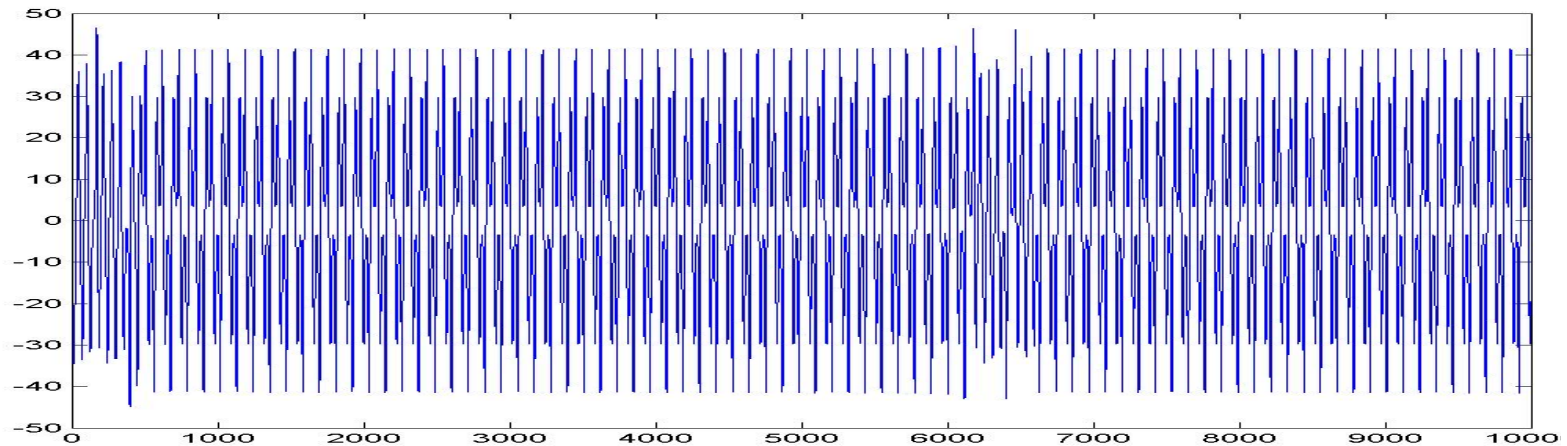


$r=165$

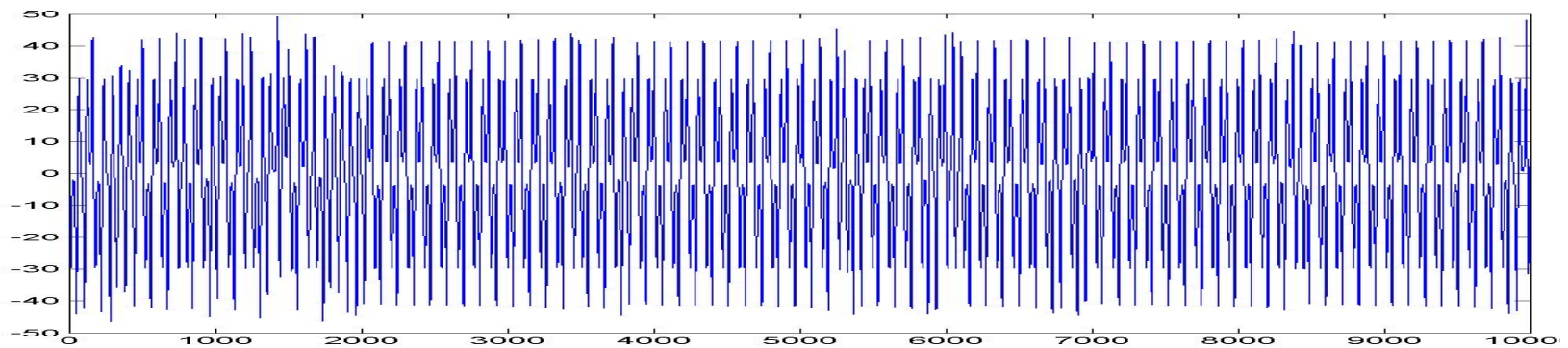


$r=166$

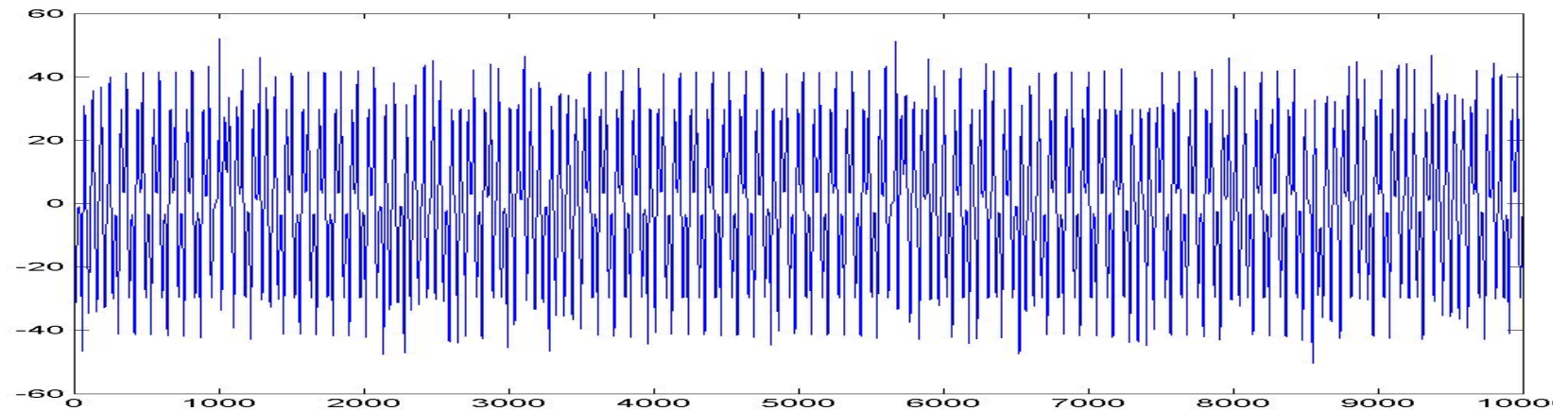
Rota para o Caos Intermitênciа



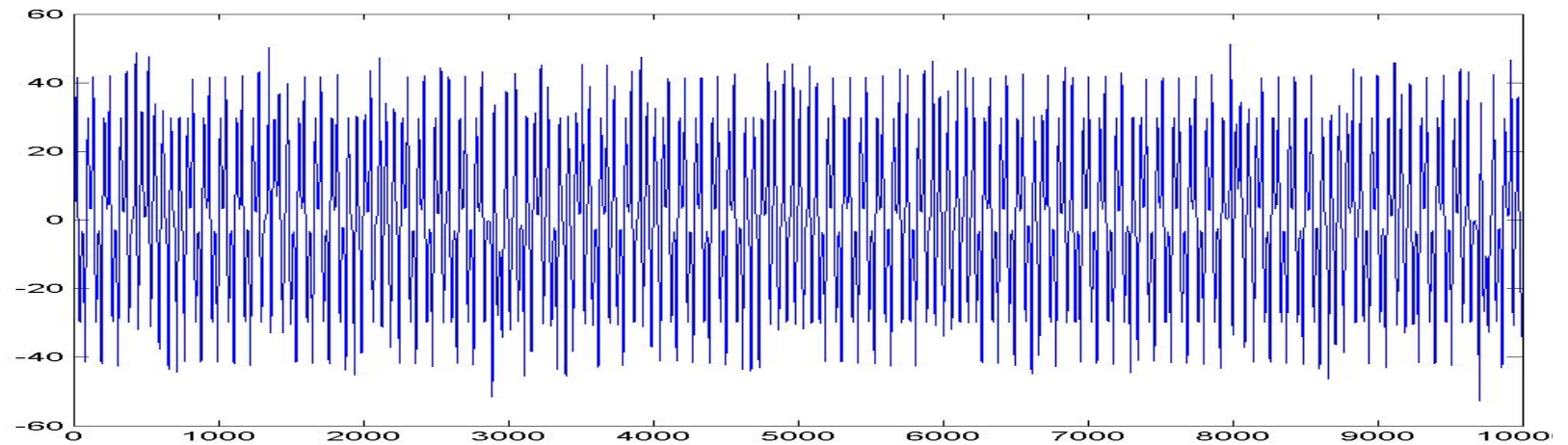
$r=166,1$



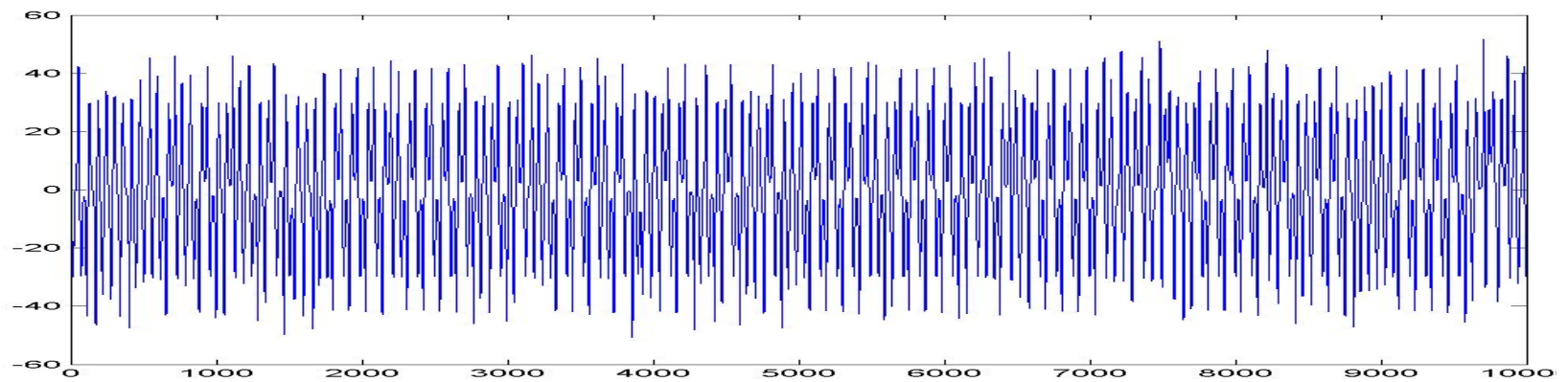
$r=166,2$



$r=166,4$

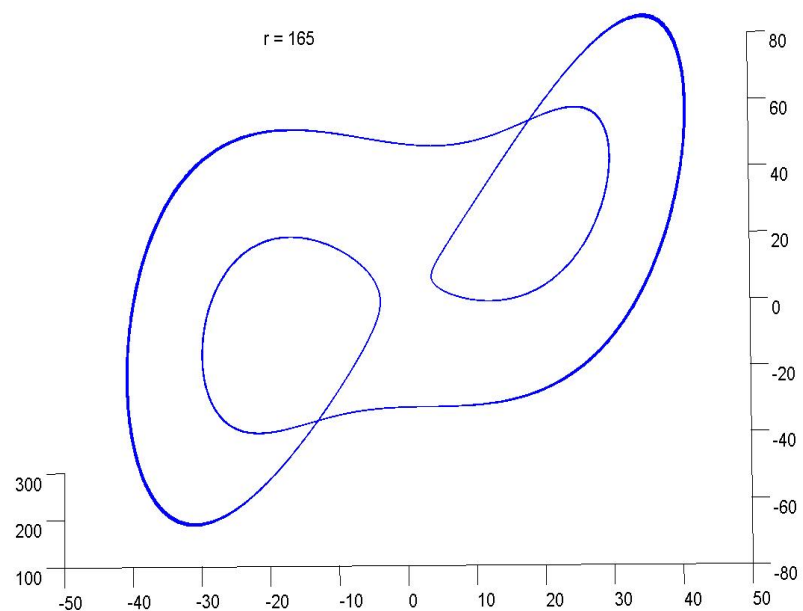


$r=166,6$

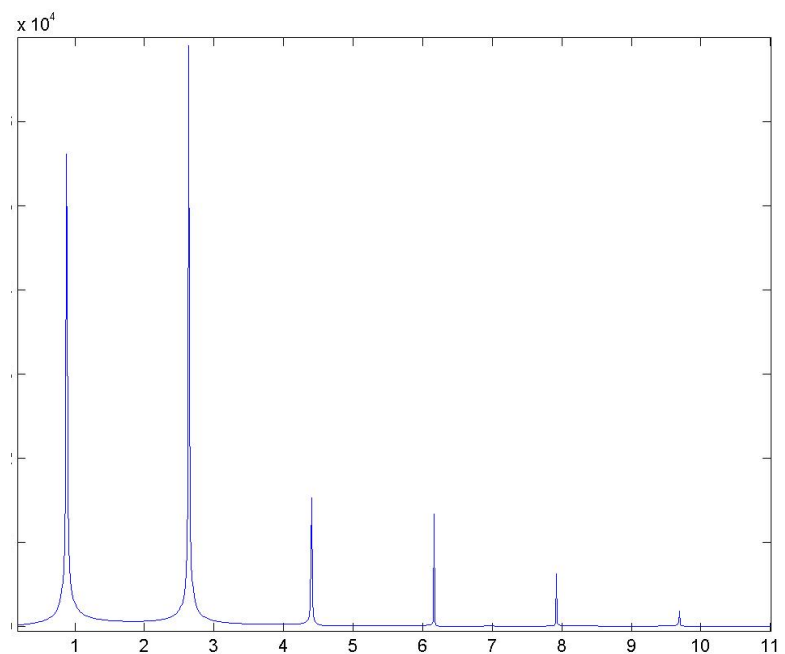


$r=166,8$

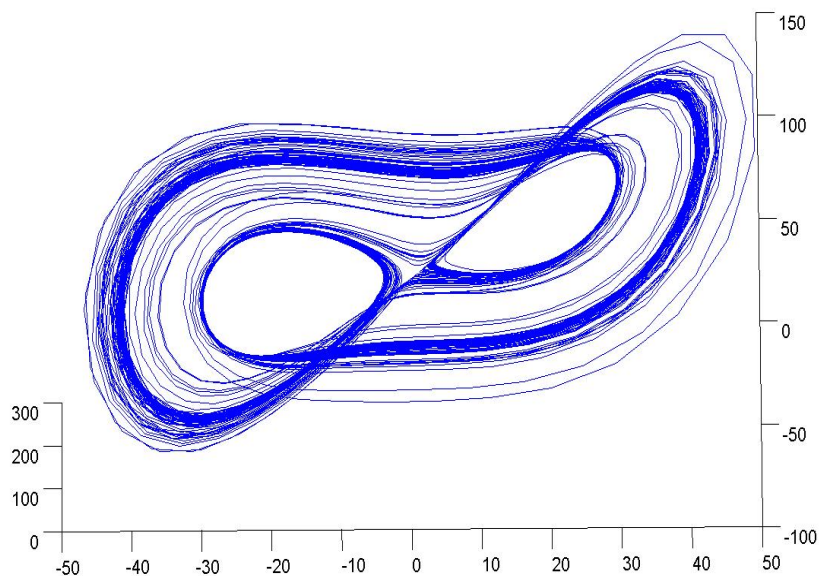
Análise Espectral Atrator Periódico



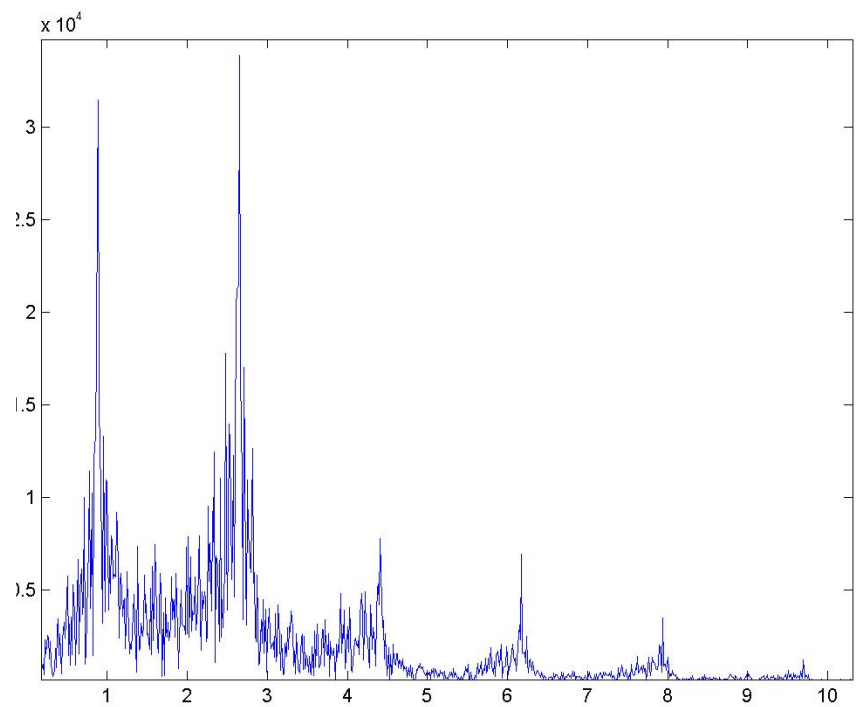
$r=165$



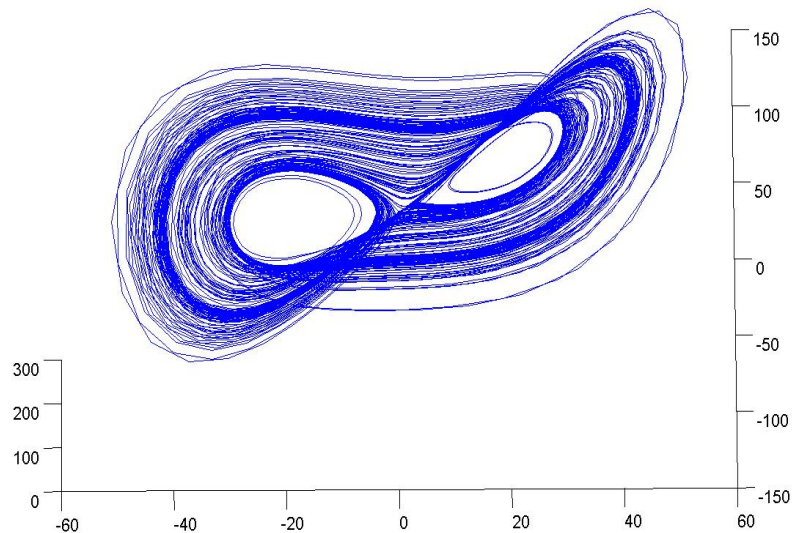
Análise Espectral Atrator Quase-Periódico



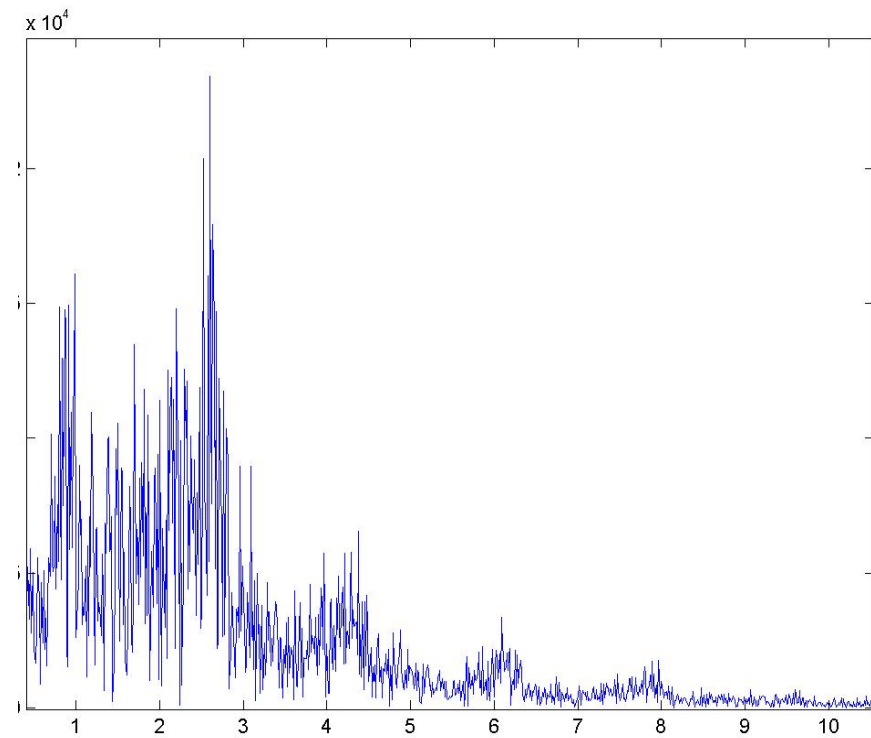
$r=166,2$



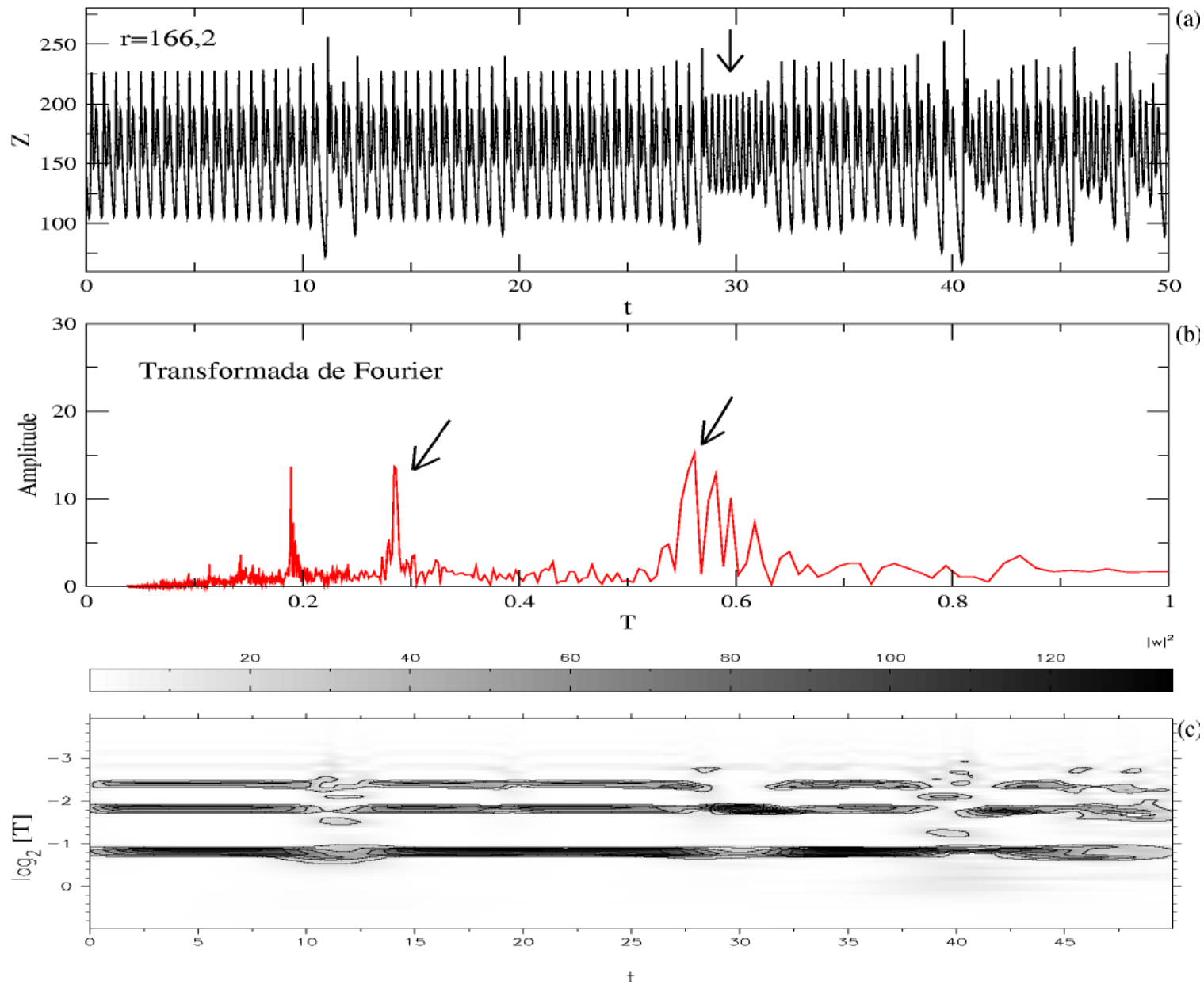
Análise Espectral Atrator Caótico



$r=166,8$

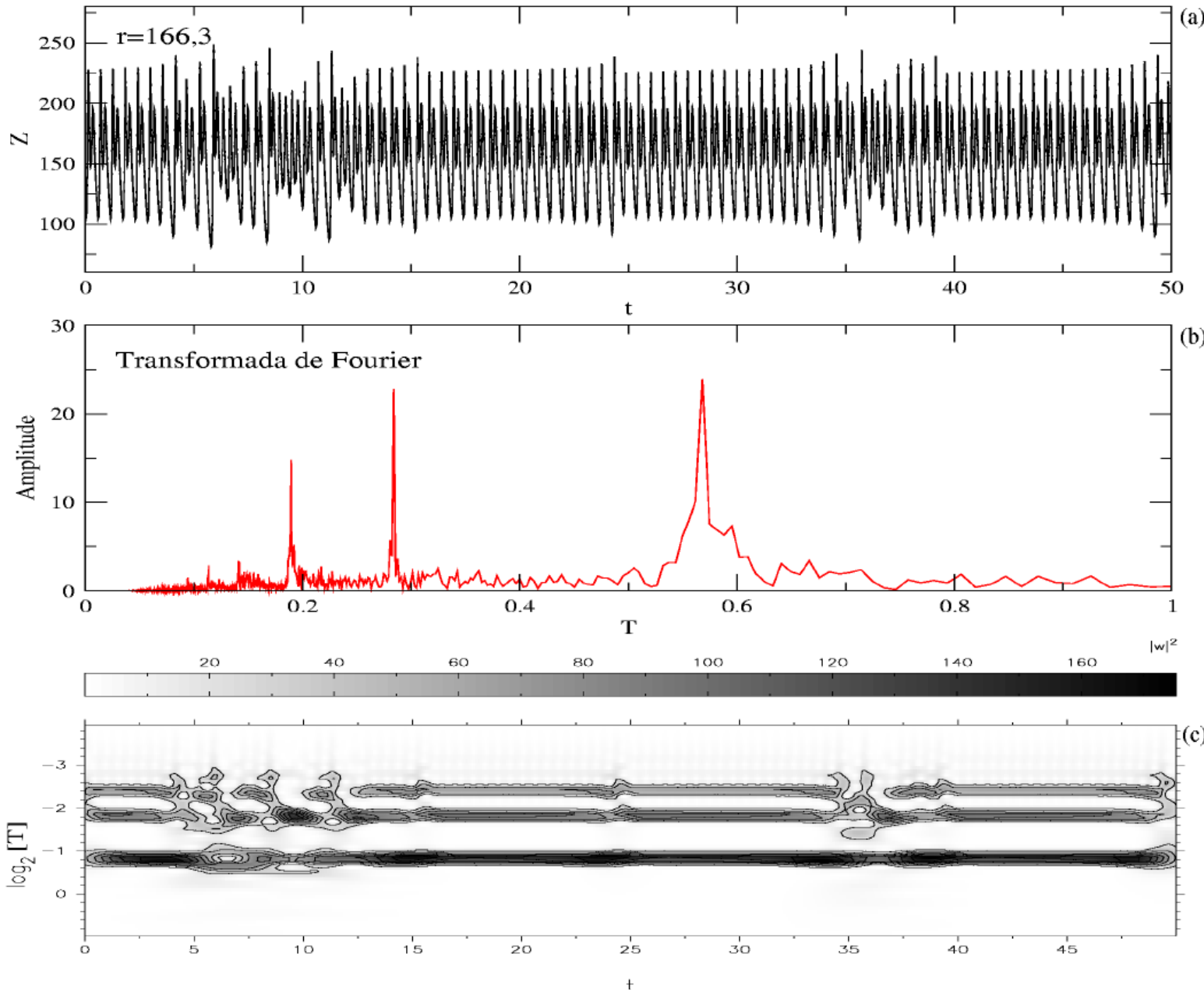


Intermitênciac no Sistema de Lorenz



Fluxos
laminar
turbulento

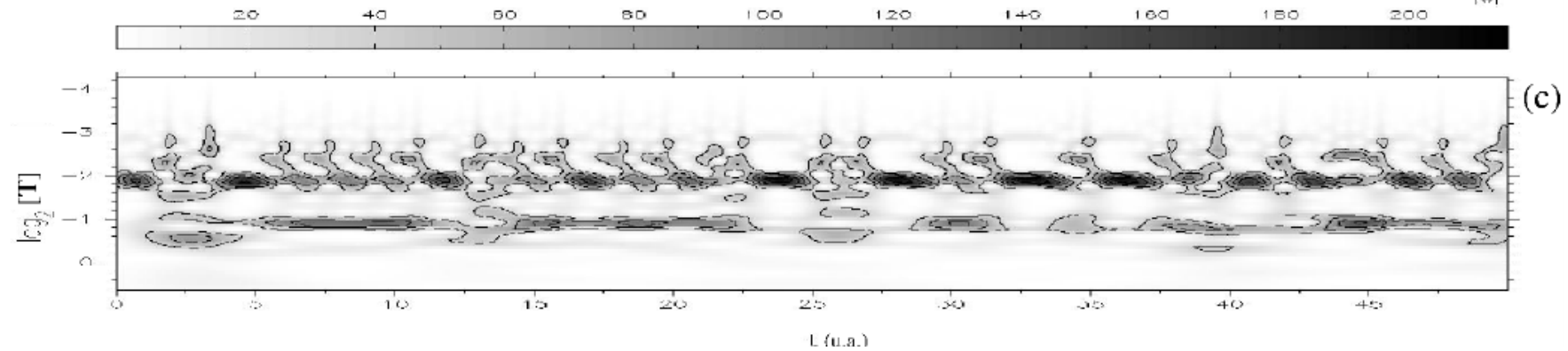
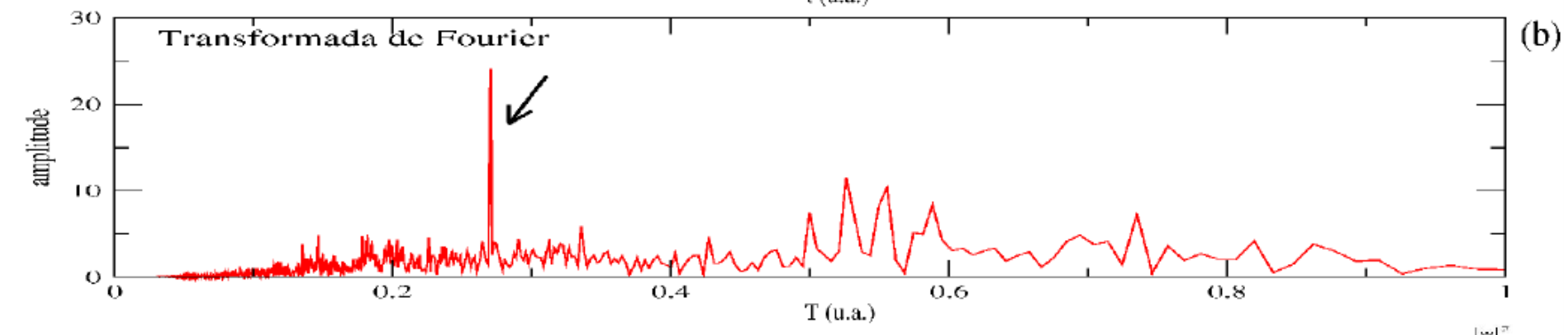
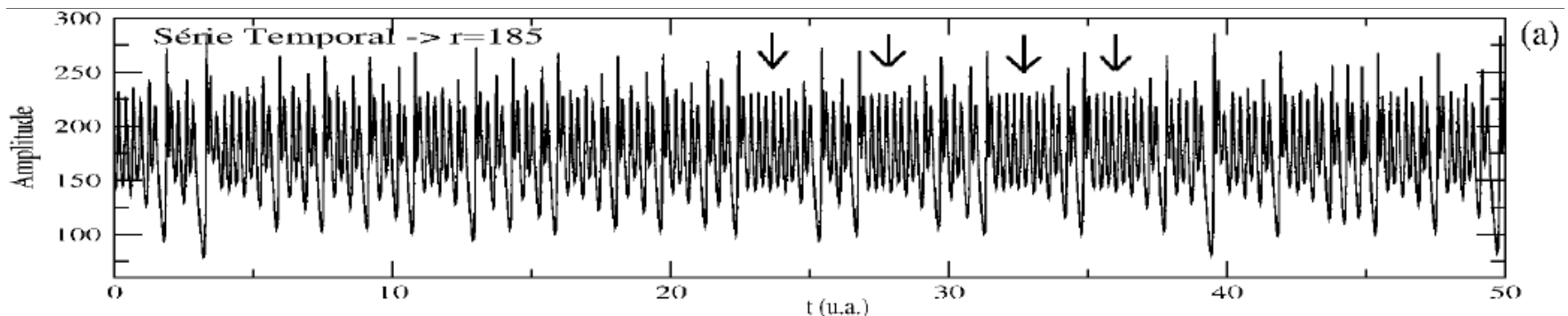
Intermitênciac no Sistema de Lorenz



Fluxos
laminar
turbulento

Intermitênci no Sistema de Lorenz

Transição irregular entre o regime laminar e o trubulento



Preturbulence: A Regime Observed in a Fluid Flow Model of Lorenz*

James L. Kaplan¹ and James A. Yorke²

¹ Department of Mathematics, Boston University, Boston, Massachusetts 02215, USA

² Institute for Physical Science and Technology and Department of Mathematics,
University of Maryland, College Park, Maryland 20742, USA

Variação de Parâmetro de Controle

- Várias rotas para o caos.
- Uma rota: caos precedido de órbita homoclínica.
- Outra rota: atrator caótico precedido de intermitência.

Intermitência = pré-turbulência

Estudo da origem da turbulência

Sistema de Lorenz

•

$$\dot{x} = -\sigma x + \sigma y$$

•

$$\dot{y} = -x y + r x - y$$

•

$$\dot{z} = x y - b z$$

Variáveis: $x, y, z \rightarrow$ espaço de fase tridimensional

Parâmetros de controle: σ, r, b

Atratores do Sistema de Lorenz

| r | Attractor |
|-----------------------|---|
| $[-\infty, 1.00]$ | $(0, 0, 0)$ is an attracting equilibrium |
| $[1.00, 13.93]$ | C_+ and C_- are attracting equilibria; the origin is unstable |
| $[13.93, 24.06]$ | Transient chaos: There are chaotic orbits but no chaotic attractors |
| $[24.06, 24.74]$ | A chaotic attractor coexists with attracting equilibria C_+ and C_- |
| $[24.74, ?]$ | Chaos: Chaotic attractor exists but C_+ and C_- are no longer attracting |

Table 9.1 Attractors for the Lorenz system (9.1).

For $\sigma = 10$, $b = 8/3$, a wide range of phenomena occur as r is varied.

Pontos fixos:

$$O = (x, y, z) = (0, 0, 0)$$

$$C = (\sqrt{b(r-1)}, \sqrt{b(r-1)}, r-1)$$

$$C' = (-\sqrt{b(r-1)}, -\sqrt{b(r-1)}, r-1)$$

$$b = 8/3 \quad \sigma = 10 \quad r > 0$$

Estabilidade do ponto O é determinada pelos auto-valores λ da matriz jacobiana

$$\begin{bmatrix} -\sigma - \lambda & \sigma & 0 \\ r & -1 - \lambda & 0 \\ 0 & 0 & -b - \lambda \end{bmatrix} = 0$$

Ponto O estável no intervalo $0 < r < 1$, pois $\lambda_i < 0$

$r > 1 \Rightarrow$ Ponto O instável $\begin{cases} \lambda_1 > 0 \\ \lambda_{2,3} < 0 \end{cases} \Rightarrow$ variedade instável unidimensional
 $\begin{cases} \lambda_1 > 0 \\ \lambda_{2,3} < 0 \end{cases} \Rightarrow$ variedade estável bidimensional

$r_s > r > 1 \Rightarrow$ Pontos C e C' estáveis, $\lambda_{1,2,3}$ reais

$$r_s > r > 1$$

C e C' atratores

Bacias atração separadas pela variedade bidimensional estável do ponto O

$$r_0 > r > r_s$$

$$\lambda_{1,2} \text{ complexos, } \operatorname{Re}\lambda_{1,2} < 0$$

C e C' atratores

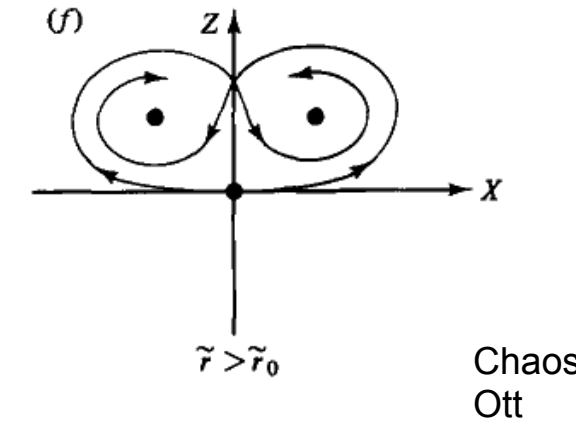
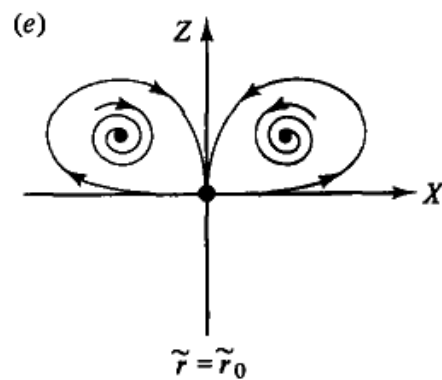
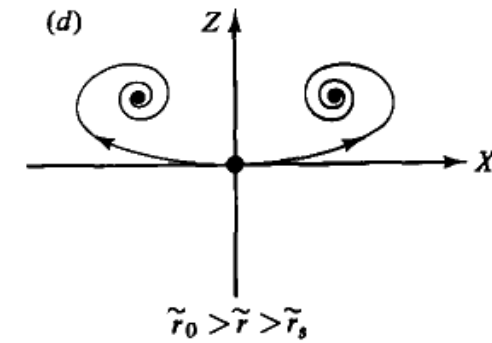
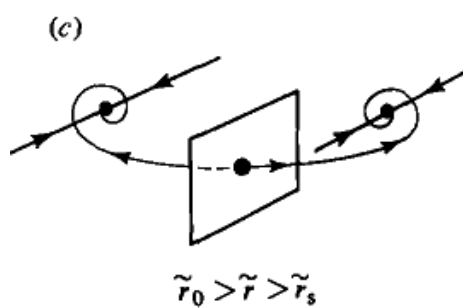
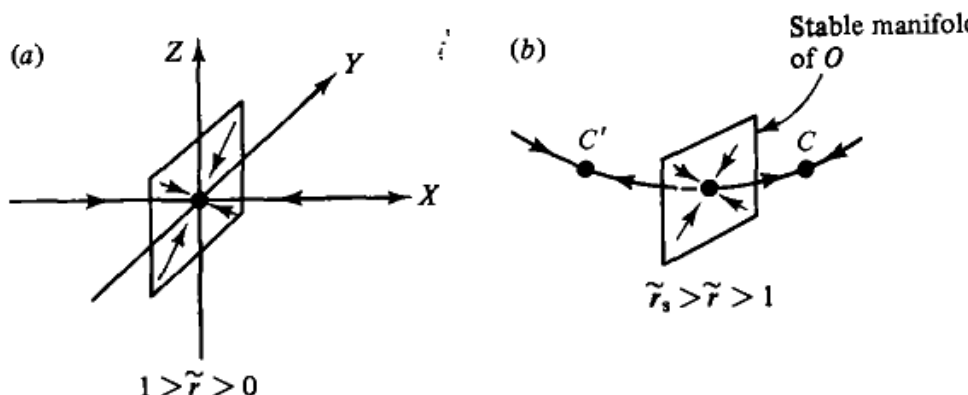
$$r = r_o = 13.93 \Rightarrow \text{Órbitas homoclínicas}$$

$$r > r_o = 13.93 \Rightarrow \text{caos transiente e caos}$$

$$\begin{cases} r < 24.06 \Rightarrow \text{transiente caótico} \\ r > 24.06 \Rightarrow \text{atrator caótico} \\ (\text{coexiste com atratores C e C'}) \\ r > 24.74 \Rightarrow \text{C e C' pontos de sela} \\ (\text{atrator caótico persiste}) \end{cases}$$

Origem do Atrator Caótico de Lorenz

- a) O ponto fixo estável
- b) O instável; C, C' estáveis
- c) O instável, C, C' estáveis
- d) Idem
- e) Órbita homoclínica
- f) Atrator caótico



Intermitênciā do Tipo 3

20. M. Dubois, M.A. Rubio, P. Bergé, "Experimental evidence of intermittencies associated with a subharmonic bifurcation," Phys. Rev. Lett. **51** (1983) 1446–1449.
21. Y. Pomeau, P. Manneville, "Intermittent transition to turbulence in dissipative dynamical systems," Commun. Math. Phys. **74** (1980) 189–197.

We report here the first observation, in a hydrodynamical system,⁷ of the so-called type-III intermittencies in the Pomeau-Manneville classification; these intermittencies arise in the process of destabilization of a limit cycle, and appear simultaneously with a period-doubling bifurcation. The turbulent bursts which appear are associated with an increase in the amplitude of the subharmonic mode.

When the Rayleigh number is increased, we observe, as in other cases,⁹ a sequence of different structures, each of them with its specific oscillators and its route to turbulence. Among these routes, we have observed the following sequence.

The onset of intermittencies corresponds to the appearance of a new unstable direction in the phase space, which, at least, is three dimensional. To point out the dynamical properties, it is useful to look at Poincaré return maps, which are best adapted to the actual experimental situation and also constitute the framework of the theoretical model.³ In a general form, these intermittencies can be described by the following relation:

$$I_{n+1} = - (1 + \epsilon) I_n + A I_n^2 + B I_n^3 + \text{higher-order terms.} \quad (1)$$

A and B are constants; ϵ is the parameter of the bifurcation; the I_n values are the successive maximum values of the relevant physical signal. In

imum values of the relevant physical signal. In order to discuss the stability of the subharmonic state, we have to apply twice the recurrent transformation, giving the following relation by keeping the most significant orders:

$$I_{n+2} = (1 + 2\epsilon)I_n + aI_n^2 + bI_n^3 \quad (2)$$

(a and b are constants). From the experimental

(a and b are constants). From the experimental data (time dependence as shown in Fig. 1), we get the I_n values as the successive maxima of the light intensity modulations seen by a photodiode. Then the return maps $I_{n+2} = f(I_n)$ are constructed. One example is given in Fig. 2: The crosses represent the (decreasing) amplitudes of the “fundamental” mode (odd n), and the squares, the (increasing) amplitudes of the “subharmonic” mode (even n), as the time evolves apart from the ghost of the fixed point (monoperiodic regime). The full curve represents the best fit by the theoretical relation (2) and has been obtained by a least-squares adjustment procedure. It yields $\epsilon = 0.098$. ϵ is expected to be proportional to the experimental control parameter $\epsilon_I = (N_{Ra} - N_{Ra,I})/N_{Ra,I}$ ($N_{Ra,I}$ is the Rayleigh number which corresponds to the threshold of the intermittent behavior).

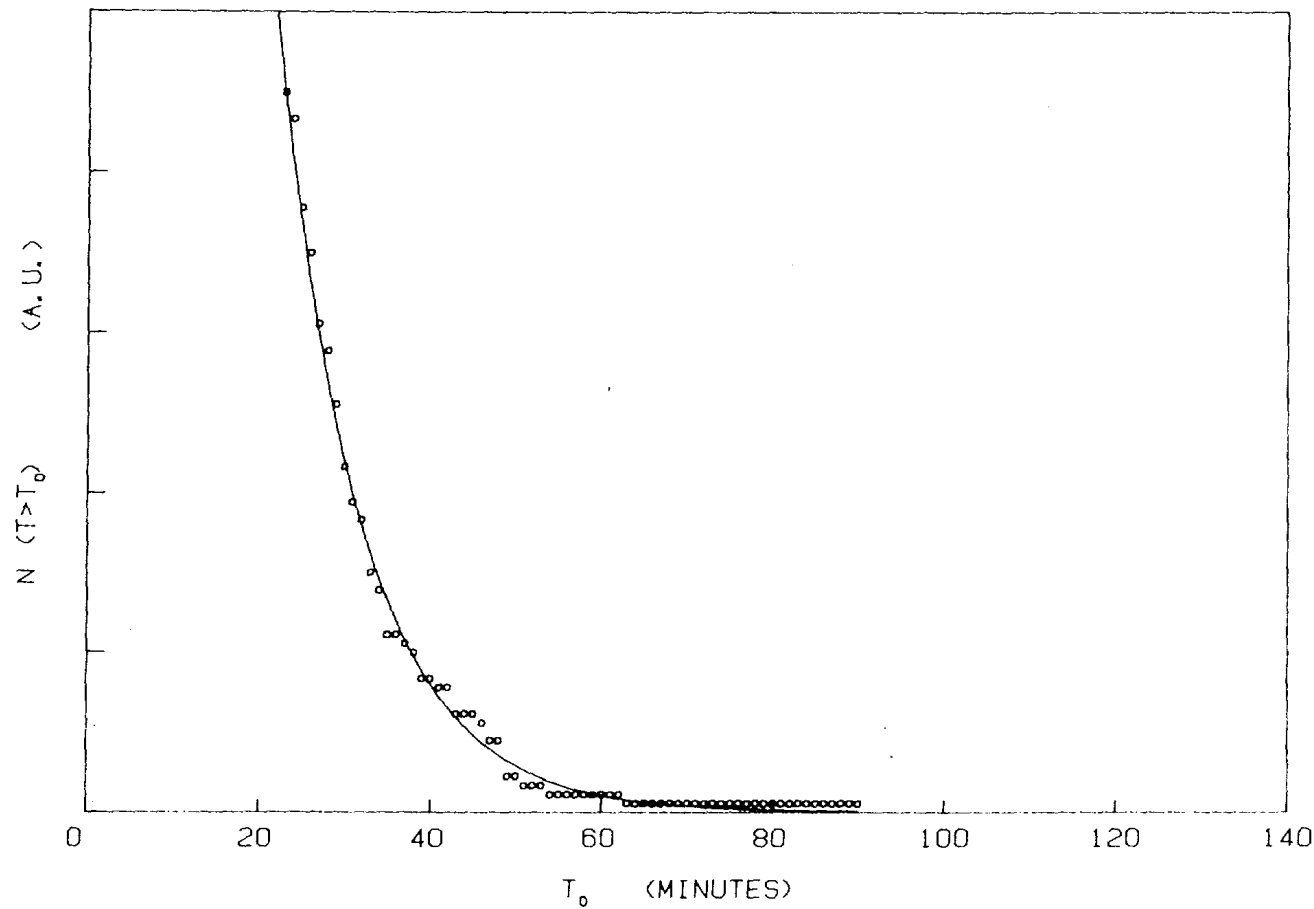


FIG. 3. Number of laminar periods with length greater than T_0 . $N_{Ra} \approx 420$. The best fit, with the relation (4), gives $\epsilon = 0.095 \pm 0.003$, in agreement with the value found from the return map (Fig. 2).

Secondary instabilities are just a step towards more complex behavior as R is increased. Different scenarios have indeed been observed, depending on the value of P . Beyond the primary instability leading to the formation of time-independent two-dimensional² rolls, time dependence was observed to introduce itself first and at relatively low R when P is small, but only after secondary instabilities adding space dependence along the rolls (three-dimensional time independent states) at large P at higher R . A compilation of early experimental results, adapted from Krishnamurti [14], is displayed in Fig. 6.

In all cases the regime called ‘turbulent convection’ was reached after a finite number of steps. At first sight this fact seemed to support the revision by Ruelle and Takens [15] of the classical Landau theory of transition to turbulence [16]: three or four bifurcations before unpredictable behavior instead of n -periodicity resulting from an infinite cascade of Hopf bifurcations. However the situation was not as satisfactory as one would have liked because the thresholds of the observed transitions were not always well defined and a residual, more or less random, component of the time dependence was most often recorded before it was decided to consider the system as turbulent. This was due to the fact that

In fact, RB convection has concentrated a large part of the efforts in the study of nontrivial features of nonlinear dynamics as applied to physical problems, namely chaos, transition scenarios, strange attractors, and the empirical reconstruction of experimental nonlinear dynamics. The main routes to chaos predicted by theory have been observed, the sub-harmonic cascade [18], the two-periodic route and its frequency lockings [19], several types of intermittency, and even less generic situations such as quasi-periodic regimes with four or five frequencies. It turns out that, while one is unable to predict which scenario will take place in a given situation, when the system is engaged in a given well-identified route, it strictly follows that route in its most intricate mathematical properties until unavoidable experimental limitations enter to blur the details.

Here is shown the example of type III intermittency [20], the intermittency that develops beyond a sub-critical sub-harmonic bifurcation. This scenario can be modeled by means of an iteration [21]:

$$X_{n+1} = -(1+r)X_n - X_n^3,$$

where X represents the amplitude of the departure from a limit cycle (corresponding to the fixed point of the iteration at $X = 0$) and r is a control parameter (negative below threshold, positive above). This local map has to be completed by a global assumption about the nature of manifold on which this reduced dynamics takes place and regarding the return of escaping iterates in the vicinity of the fixed point. Type III intermittency was observed by Dubois *et al.* [20] in convection using silicone oil (large P). A typical time series is displayed in Fig. 7 (top). Displayed on the bottom line of that figure, the return maps of the maxima I_n of some observable plotted every two determinations, i.e. I_{n+2} as a function of I_n and the statistics of the durations of closely periodic sequences before escape—the so-called laminar intermissions—both agree quantitatively with corresponding theoretical predictions after appropriate empirical rescaling.

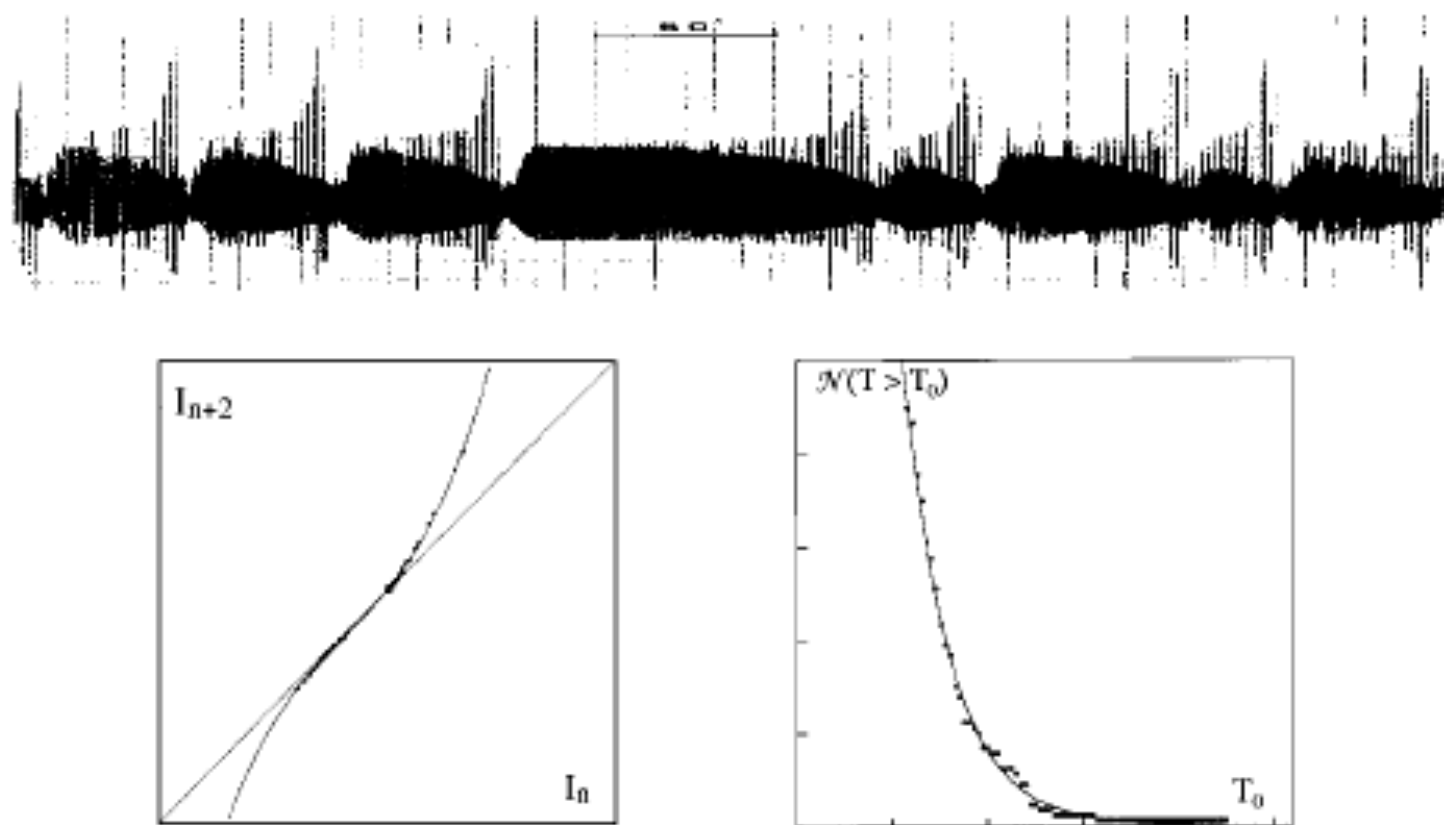


Fig. 7. Type III intermittency in RB convection after Dubois *et al.* [20]. Top: time series of a velocity component measured at some point in the cell. Bottom-left: effective iteration obtained by displaying maxima of that variables every two steps. Bottom-right: cumulative distribution function of the duration of laminar intermissions.

Transição Via Quase-Periodicidade

Recall that there are 3 generic ways in which a limit cycle on a Poincaré map may become unstable: An eigenvalue λ of the Floquet matrix (the Jacobian of the map) crosses the unit circle at

- $+1$ (as in the example of intermittency above);
- -1 (as we saw in the introduction to period doubling); and
- $\lambda = \alpha \pm i\beta$, $|\lambda| > 1$. This corresponds to the transition via *quasiperiodicity*.

As we have seen, the latter case results in the addition of a second oscillation.

This is a *Hopf bifurcation*: the transformation of a limit cycle to a quasiperiodic flow, or a torus T^2 .

The route to chaos via quasiperiodicity describes how a torus T^2 (i.e., a quasiperiodic flow) can become a strange attractor.

III – Fluido em Rotação

- Água entre dois cilindros.
- Cilindro interno em rotação. Cilindro externo em repouso.
- Transição para turbulência.
- Parâmetro de controle: velocidade de rotação do cilindro interno.

Onset of Turbulence in a Rotating Fluid*

J. P. Gollub†‡ and Harry L. Swinney

Physics Department, City College of the City University of New York, New York, New York 10031

(Received 17 July 1975)

Light-scattering measurements of the time-dependent local radial velocity in a rotating fluid reveal three distinct transitions as the Reynolds number is increased, each of which adds a new frequency to the velocity spectrum. At a higher, sharply defined Reynolds number all discrete spectral peaks suddenly disappear. Our observations disagree with the Landau picture of the onset of turbulence, but are perhaps consistent with proposals of Ruelle and Takens.

relation functions). Specifically, we have studied the radial velocity in a fluid rotating between concentric cylinders. The observed behavior clearly contradicts the Landau model of the onset of turbulence.

In our experiments the fluid (water) was confined between an inner rotating stainless-steel cylinder of radius $r_1 = 2.224$ cm and a stationary precision-bore glass tube of inner radius $r_2 = 2.540$ cm. The gap d was uniform to within 1% over its entire length. The fluid height in the cell The local radial velocity V_r was observed by an optical heterodyne technique using an optical arrangement described elsewhere.⁸ The scattering

The local radial velocity V_r was observed by an optical heterodyne technique using an optical arrangement described elsewhere.⁸ The scattering volume was located at the center of the gap between the cylinders, and its largest dimension was 150 μm , about 0.05 of the gap. Thus the observations are essentially local measurements, and no significant spatial averaging is involved. The time-dependent frequency of the photocurrent measured for 1024 adjacent sampling intervals of 5×10^{-4} to 5×10^{-1} sec.

In the discussion to follow the rotation rate is expressed in terms of a reduced Reynolds number $R^* = R/R_T$, where $R = 2\pi r_1 d / \nu T$ (ν is the kinematic viscosity) and $R_T = 2501$ is the value of R at the onset of aperiodic motion.

We now describe the sequence of transitions which are observed reversibly as R is varied. The first instability (the Taylor instability) occurs at $R^* = 0.051$, and results in a time-independent toroidal roll pattern that has been extensively studied.⁴⁻⁸ The radial velocity is periodic in the axial coordinate z , with wavelength 0.79 cm.

The first transition to a periodic state occurs at $R^* = 0.064$, where transverse waves (with four wavelengths around the annulus) are superimposed on the toroidal vortices.⁹ These waves, which have been previously observed visually,⁴ manifest themselves as an oscillation at a frequency f_1 in our measurements, as shown in Fig. 1(a) for $R^* = 0.504$. The frequency f_1 scales with

When R^* is increased to 0.54 ± 0.01 , a second time-dependent instability occurs, and a new frequency f_2 is visible as a low-frequency modulation of the radial velocity [Fig. 1(b)]. The corre-

90% of the power, remain sharp. A new frequency f_3 (and its harmonics) appears at $R^* = 0.78 \pm 0.03$, and this is also visible in Fig. 1(c). Note that f_3 appears only after f_2 has disappeared.

Oscilações na Água entre Dois Cilindros

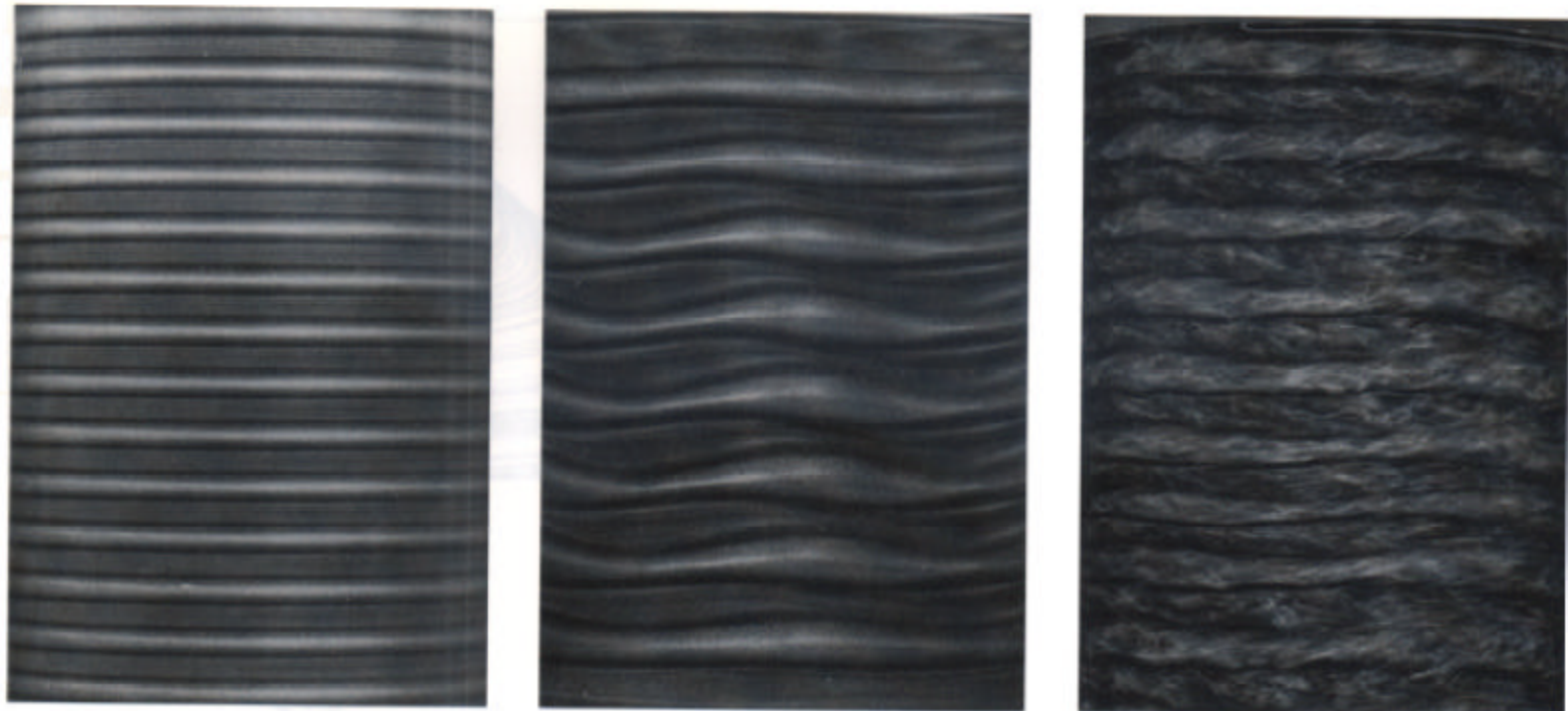


FIGURE 1. Patterns formed in water contained between concentric cylinders with the inner cylinder rotating: *a* steady pattern of stacked donut-shaped rolls. *b* waves on the rolls. *c* chaotic flow. The patterns are made visible by adding a small amount of flat flakes (often ground up fish scales) that align with the flow.

Espectros das Flutuações

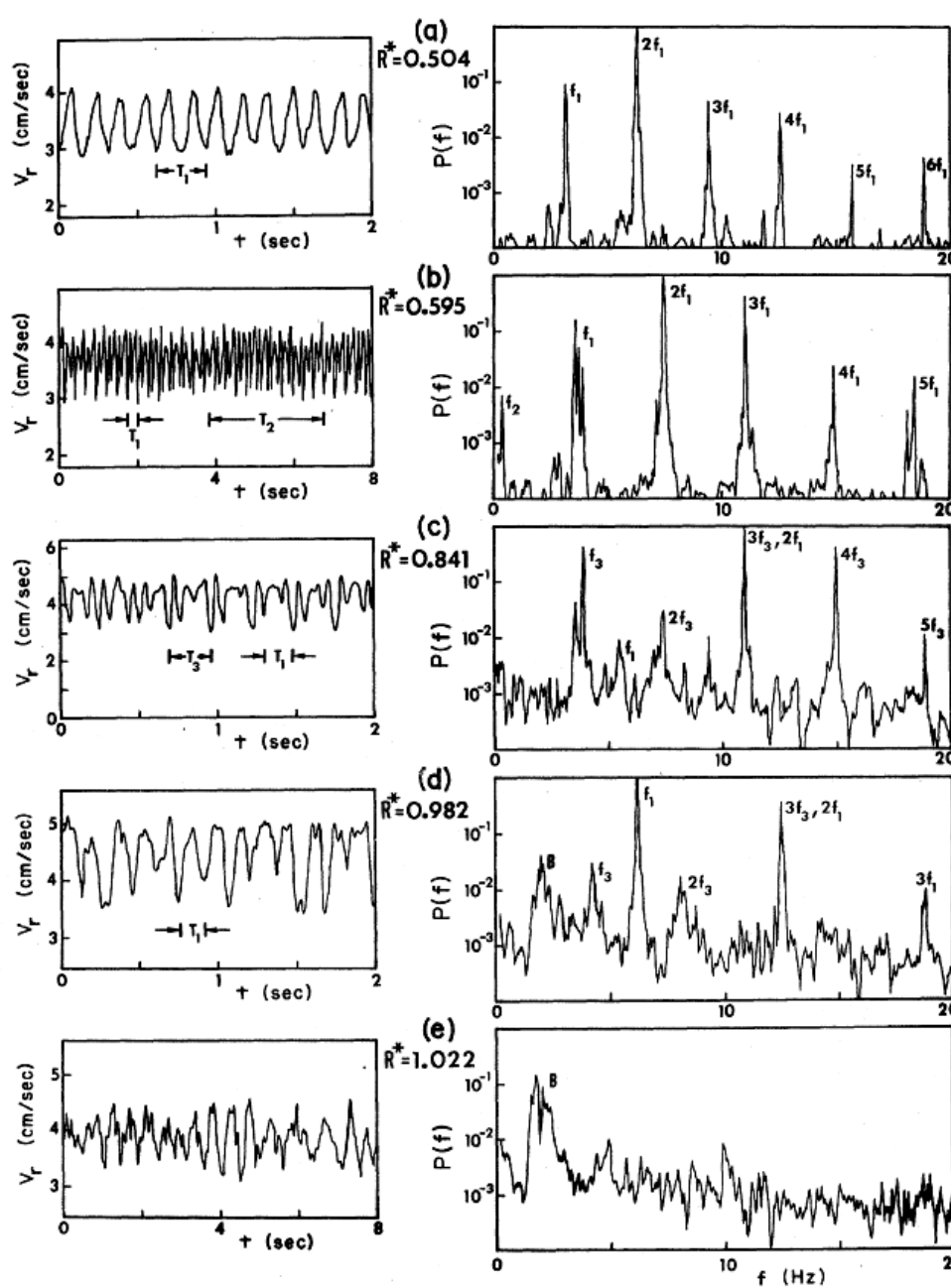


FIG. 1. Time dependence of the radial velocity and corresponding power spectra $P(f)$ [with units $\text{cm}^2 \text{ sec}^{-2} \text{ Hz}^{-1}$, normalized so that $\int_0^{25 \text{ Hz}} P(f) df = \langle (\Delta V_r)^2 \rangle$] for different reduced Reynolds numbers $R^* = R/R_{T^*}$.

Modos Observados

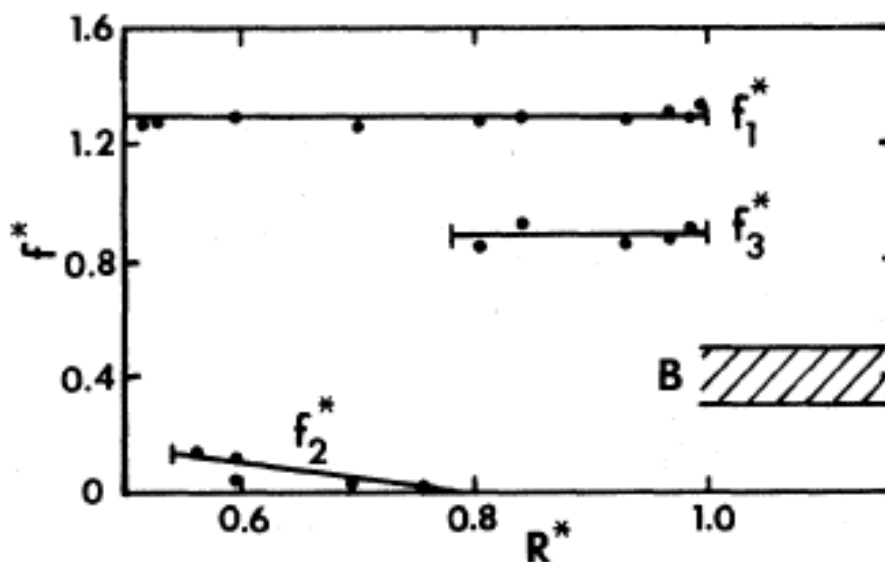


FIG. 2. The dimensionless frequencies $f_i^* = f_i T$ as a function of R^* . The solid lines are to guide the eye, and the vertical bars demarcate the regions in which the f_i are present (except that the lower bound for f_1 is $R^* = 0.064$). The fact that $f_1^* = 1.30$ and $f_3^* = 0.87$ are constant indicates that f_1 and f_3 scale with rotation rate, whereas f_2 does not.

V – Reação Química

Aspectos dinâmicos descritos por um mapa unidimensional

Roux, J.-C., Simoyi, R.H., Swinney, H.L., “Observation of a strange attractor”. *Physica D* **8**, 257-266 (1983).

Coffman, K.G., McCormick, W.D., Noszticzius, Z., Simoyi, R.H., Swinney, H.L., “Universality, multiplicity, and the effect of iron impurities in the Belousov-Zhabotinskii reaction.” *J. Chemical Physics* **86**, 119-129 (1987).

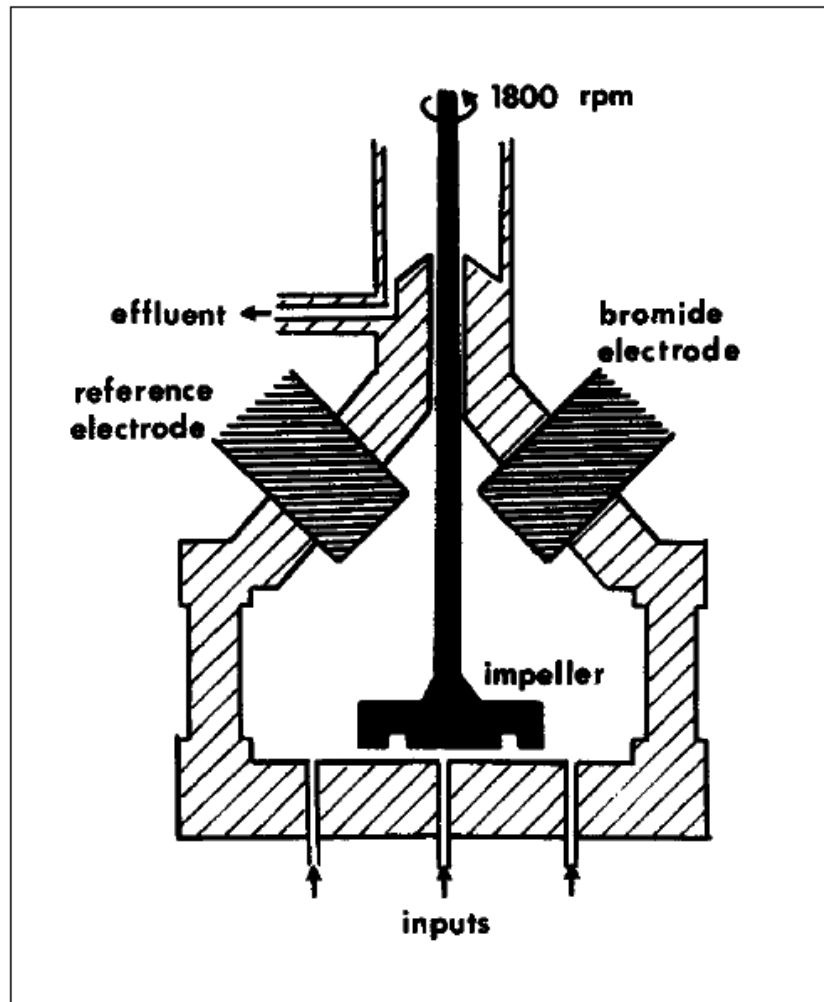


Figure 3.17 A schematic diagram of the chemical reactor used for the BZ reaction.

The volume of the cylindrically symmetric chamber is 33 cc.

Tipos de Oscilações

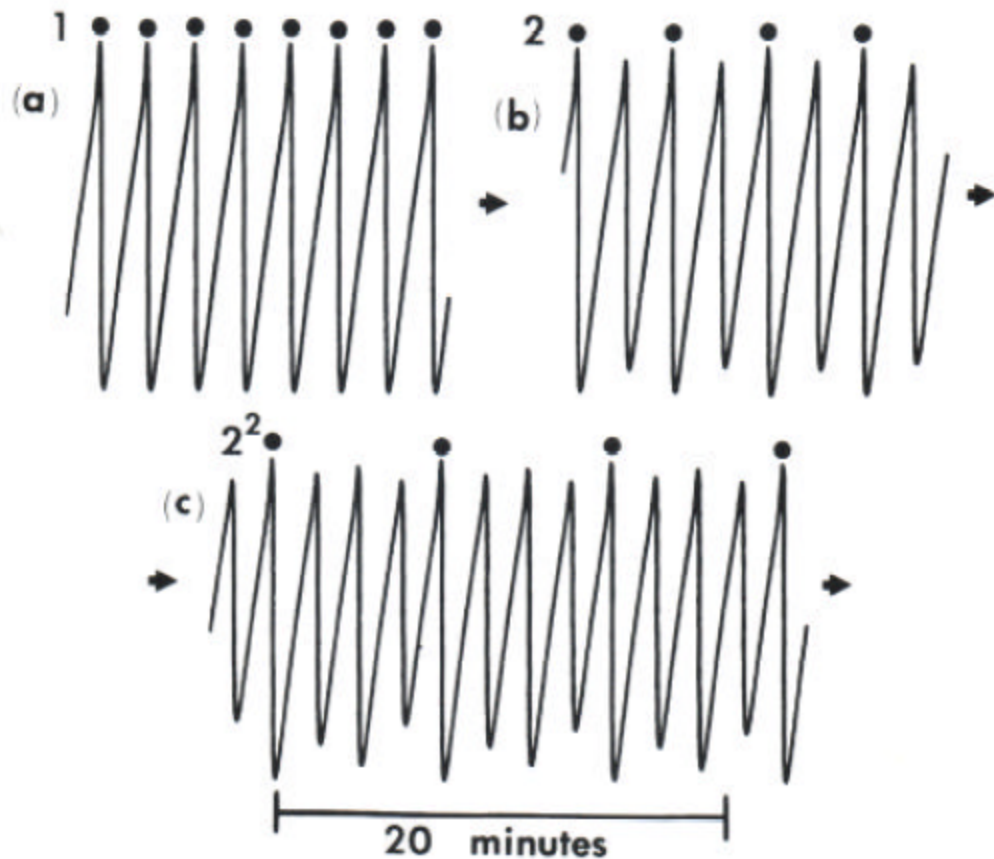
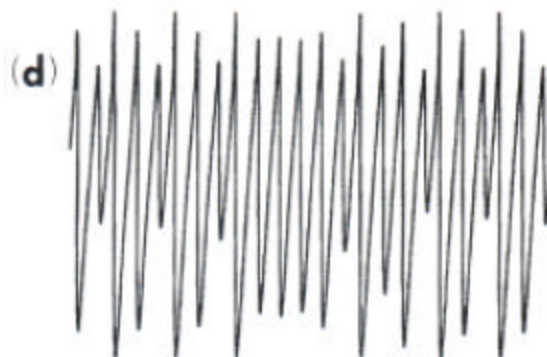


FIGURE 2. Measurements of the time dependence of the concentration of one of the chemical species produced by a chemical reaction: *a*, periodic oscillations. *b*, oscillations with double the original period. *c*, oscillations with four times the original period. *d*, chaotic oscillations. The dots above the periodic waveforms are separated by one period.



Atratores

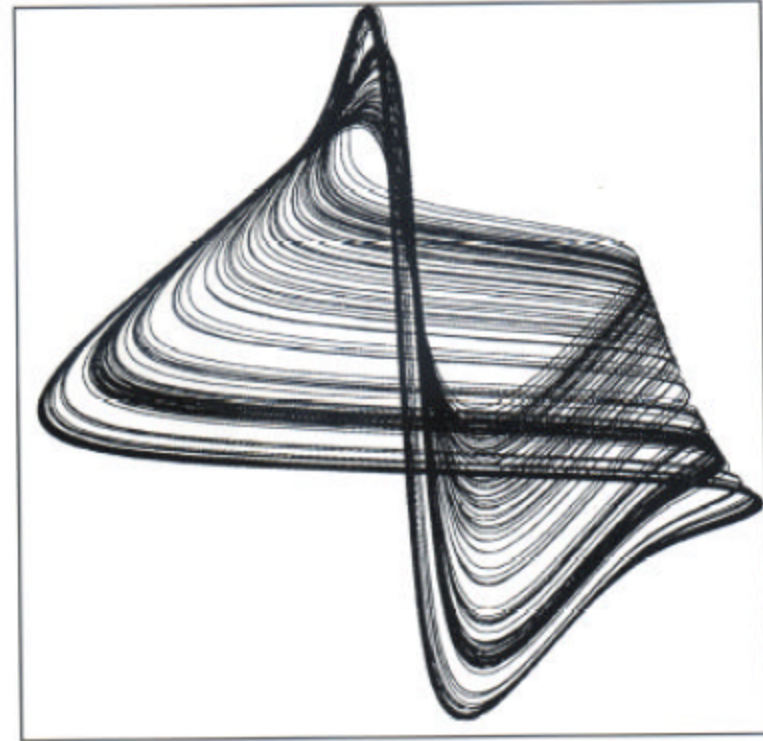
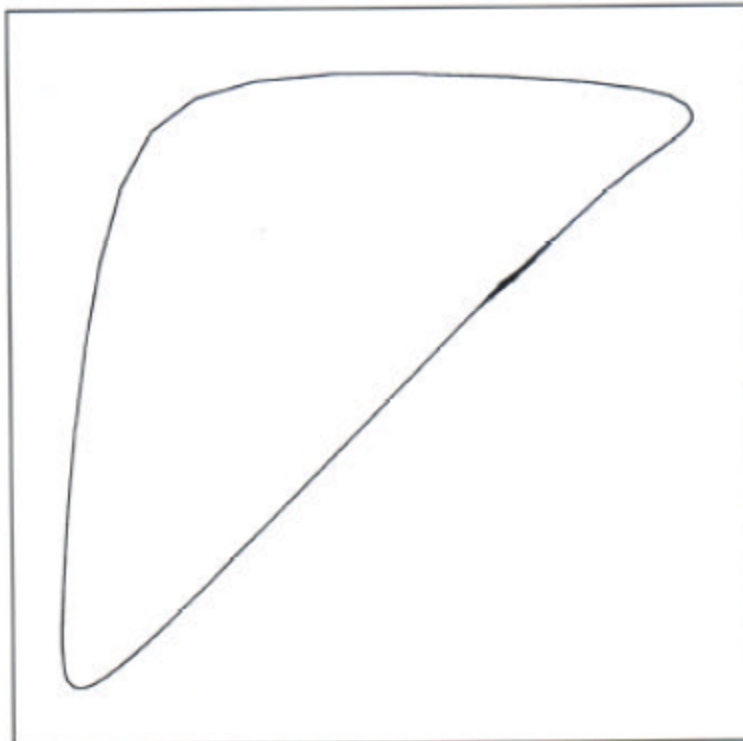


FIGURE 3. Abstract portraits of the behavior of a chemical reaction: *a*, periodic oscillations. *b*, chaotic oscillations.

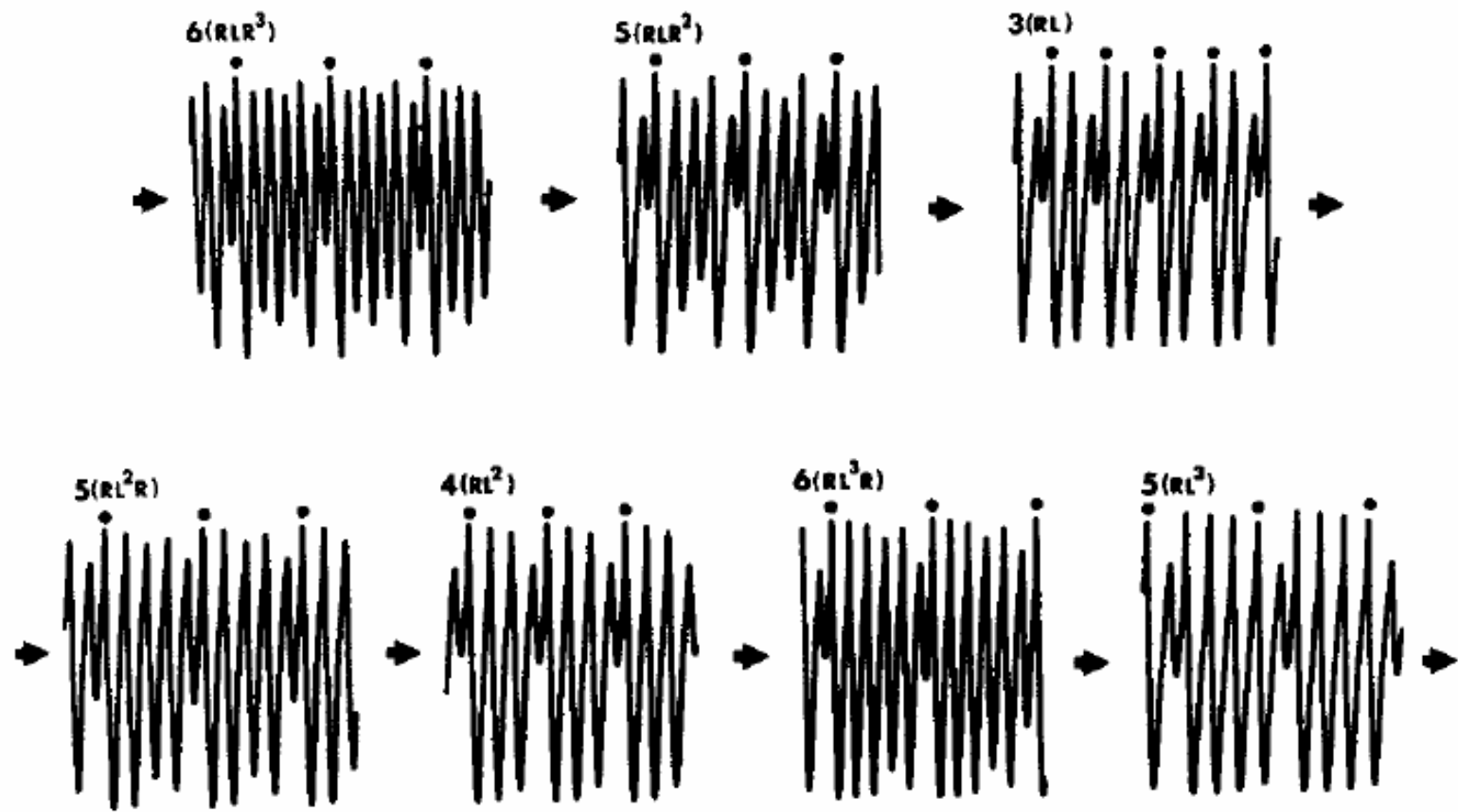


Figure 3.18 Periodic oscillations of the bromide concentration.

The horizontal axis is time, and the concentration is graphed vertically. Dots are shown to mark the period of the oscillation.

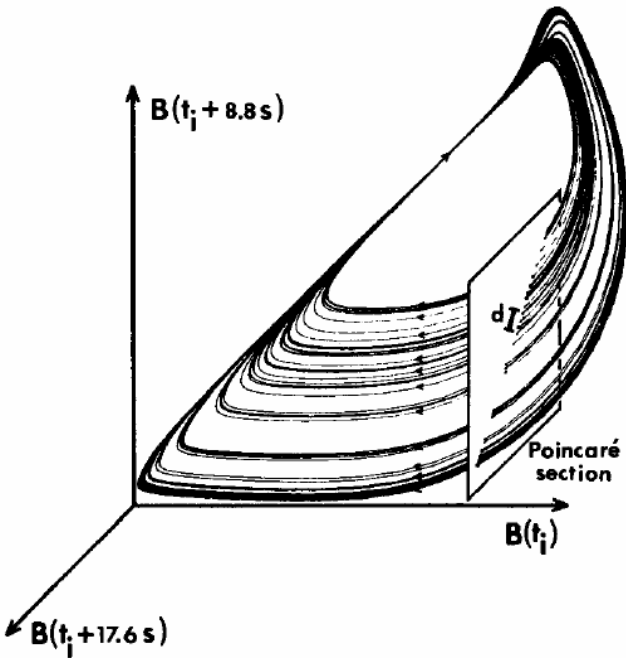


Figure 3.19 Reconstruction of dynamics from the bromide time series.

The three coordinates are the concentrations at three equally spaced time intervals.

The Poincaré section, shown as a plane, intersects the data essentially in a curve, which allows a reduction to the one-dimensional map of Figure 3.20.

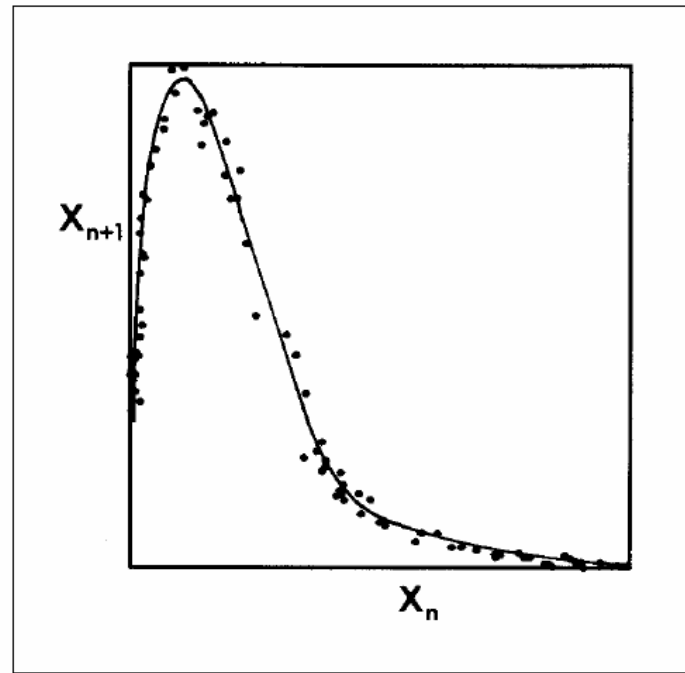


Figure 3.20 One-dimensional map reconstructed from the time series.

A spline fit was made to the data points from Poincaré map of Figure 3.19.